Ground-Space Observations of Pc5 Poleward Moving Auroral Arc Pulsations and Field-Line Resonances in the Post-Midnight Sector: THEMIS Observations

Natsuo Sato (nsato@nipr.ac.jp)
National Institute of Polar Research https://orcid.org/0000-0003-2499-310X
Akira Sessai Yukimatu
National Institute of Polar Research Division for Research and Education: Kokuritsu Kyokuchi Kenkyujo Kenkyu Kyoikukei
Yoshimasa Tanaka
National Institute of Polar Research
Tomoaki Tomoaki
Nagoya University
Akira Kadokura
National Institute of Polar Rearch

Full paper

Keywords: auroral arc, Pc5 pulsation, field-line resonance, pulsating aurora, all-sky imager, THEMIS, field-aligned current, field-aligned electric field, magnetosphere-ionosphere coupling

Posted Date: September 16th, 2020

DOI: https://doi.org/10.21203/rs.3.rs-73470/v1

Abstract

We investigate the Pc5 poleward moving auroral arc (PMAA) pulsations (~ 4–5 min period) using the ground-based all-sky imager network and the Time History of Events and Macroscale Interactions during Substorms (THEMIS) A, D, and E satellites, whose footprints were located near the PMAA in the post-midnight sector. The Pc5 PMAA pulsations considered herein occurred in conjunction with the enhancement of the magnetic and electric field oscillations observed near the equatorial plane of the magnetosphere. The magnetospheric oscillation signal displayed three-cycle oscillations, which correspond primarily to the PMAA pulsations. The value of coherence between the magnetospheric oscillations and the luminosity pulsations was higher than 0.9. Based on these observations, it is suggested that the PMAA pulsations and the magnetospheric field oscillations are initiated by the same physical mechanism and thus oscillate concurrently by the magnetosphere-ionosphere (M-I) coupling. The satellite data indicated a longer period of magnetospheric oscillations at the higher latitude site. On the other hand, the measured period of the PMAA pulsation was almost constant in the lower latitude region (~ 68.5°-70.0° MLAT), whereas in the higher latitude region (~ 70.0°-70.5° MLAT) it increased with increasing latitude. This signature demonstrates that the oscillations on the lower latitudinal side of the PMAA conformed with the monochromatic frequency field-line resonance (FLR) where the oscillation period was constant and independent of latitude, whereas the higher latitude side of the PMAA presented a multi-frequency FLR region where the period lengthened with increasing latitude. The Pc5 magnetic pulsations observed on the ground neither exhibited a clear coincidence with the PMAA pulsations nor with the magnetospheric magnetic oscillations. On the other hand, the H component of magnetic pulsations demonstrated a rather similar behavior to that of the ion pressure variation within the magnetosphere. The solar wind speed was significantly high, approximately 650 km/s, during this event. The magnetospheric magnetic and electric field oscillations could be triggered simultaneously in a wide region by an impulse such as rapid convection changes caused by the sudden variations of the interplanetary magnetic field (IMF) Bz, which was observed by the SuperDARN radar and the Geotail satellite.

1. Introduction

There are two types of auroral luminosity pulsations. The first type is a short-period pulsation with the main period of a few to a few tens of seconds, which is called pulsating aurora (see the review by Lessard, 2012), and is mainly observed during the recovery phase of a substorm. The second type is a longer period pulsation in the Pc5 (150–600 s) period range, which is called long-period auroral pulsation. The long-period auroral pulsations have two categories: one is arc aurora luminosity pulsation and the other is a patch aurora luminosity modulation. Previous studies reported that long-period auroral arc pulsations have a good correlation with Pc5 magnetic pulsations and their latitudinal amplitude and phase relation is consistent with the FLR models (Chen and Hasegawa, 1974; Southwood, 1974; Xu, et al., 1993; Samson et al., 1996, 2003; Milan et al., 2001; Baddeley et al., 2017). Such evidence suggests that the auroral arc may be related to the field-aligned current associated with the FLRs (Milan et al., 2001;

Samson et al., 2003; Tanaka et al., 2012; Gillies et al., 2018). These physical processes are not well understood yet. On the other hand, the long period modulation of a diffuse patch aurora, including pulsating aurora is thought to be caused by the electron pitch-angle scattering with compressional mode Pc5 pulsations (Oguti et al., 1987; Yamamoto, 1988; Saka et al., 2014).

In this study, we examine the characteristics of arc type long-period auroral pulsations. Long-period auroral pulsations have been observed not only from the ground (Samson et al., 1996, 2003, Milan et al., 2001; Tanaka et al., 2012; Saka et al., 2014; Baddeley et al., 2017 and Gillies et al., 2018) but also from space (Liou et al., 2008; Liou and Takahashi, 2013; Liou and Sibeck, 2014, 2018). Gillies et al. (2018) examined the statistical data on auroral pulsations. They showed that optical redline (630 nm) auroral arc pulsations occur most frequently near 20 and 04 magnetic local time (MLT).

The space-ground coordinated observations using high spatial/temporal resolution data can provide important information concerning the long-period Pc5 auroral arc pulsations associated with FLR oscillations. However, to the best of our knowledge, there are no reports of such space-ground coordinated observations. Our motivation to study the long-period Pc5 auroral arc pulsation in the post-midnight sector stemmed from our former work. During our previous observations of pulsating auroras and omega bands (Sato et al., 2015 and 2017) using the dataset compiled by the THEMIS ground-based all-sky imager network, we found clear evidence of long-period Pc5 auroral arc pulsation events in the post-midnight sector at the higher latitude region of the pulsating aurora. Therefore, we focused our current study on the Pc5 auroral arc pulsations observed in the post-midnight sector.

The data were observed by the THEMIS ground-based all-sky imager network in this study. Using the data, we could pick up the fortunate events whereby the footprints of the THEMIS-A (TH-A), THEMIS-D (TH-D), and THEMIS-E (TH-E) spacecraft (using TS05 model [Tsyganenko & Sitnov, 2005]), whose orbits were located near the equatorial plane of the magnetosphere, traversed the field of view of the all-sky imager and the Pc5 auroral arc pulsations were observed during the interval of 1210–1240 UT on 2nd March 2011.

In this study, we refer to the long-period auroral arc pulsations as "Pc5 poleward moving auroral arc (PMAA) pulsations," which were previously used by Kozlovsky and Kangas (2002) and Tanaka et al., (2012). They referred to it as PMAA to distinguish these phenomena from the poleward moving auroral forms (PMAFs) (Sandholt et al., 1990) that are observed in the dayside cusp region and are caused by the solar wind-magnetosphere reconnection. Here, we report on the observational evidence of the Pc5 PMAA pulsation signals and the magnetospheric magnetic and electric field oscillations through the ground-space coordinated observations.

2. Instrumentation

In this study, we use optical all-sky imagers (ASIs) and magnetometers of the THEMIS ground-based observatories (GBO) [Angelopoulos, 2008; Mende et al., 2008]. We also use particles and field data

obtained onboard TH-A, TH-D, and TH-E spacecraft from the electric field instrument [Bonnell et al., 2008], electrostatic analyzer [McFadden et al., 2008], and fluxgate magnetometer [Auster et al., 2008].

The coordinated THEMIS/ASIs observations provided auroral images covering broad latitude and longitude (~ 1000 km) ranges with high spatial (~ 1 km near zenith) and temporal (3 s) resolutions. The white light imagers cover a wide wavelength band of ~ 400–700 nm, and the images were projected onto an ionospheric altitude of 110 km. We also use ground magnetometer data with a 0.5 s time resolution. To examine the morphological and dynamic signals of the shapes and motions of Pc5 PMAA pulsations, we produced movie files using the original 3-s-resolution ASIs data.

3. Observations

3 − 1. Selection of Pc5 PMAA pulsation event

To identify “Pc5 PMAA pulsation” events in this study, we first examined a summary plot of the THEMIS data (for example, that of the March 2, 2011, <http://themis.igpp.ucla.edu/summary.php?year=2011&month=03&day=02&hour=0024&sumType=asi&type=keograms>). Our selection method is based on qualitative visual inspection of the images. Pc5 PMAA pulsation-like events can be identified in the keogram because most of them display a “repeated poleward moving” structure. Subsequently, we analyzed the auroral shapes using a sequence of ASI images to verify whether the shapes of the auroras resembled an auroral arc. Finally, we selected 119 events during a five-year period from January 2007 that exhibited the specific characteristics of Pc5 PMAA pulsations.

3 − 2. Ground-space coordinated observations of Pc5 PMAA pulsations

We examine the fortunate event that occurred when the footprints of the THEMIS spacecraft were located very close to the Pc5 PMAA pulsations region observed from the ground during the period 1210–1240 UT on 2nd March 2011.

3-2-1. Ground-based observations of Pc5 PMAA pulsations

The upper panel (a) of "Figure 1" shows the keogram observed at Fort Smith (FSMI). The geographic and geomagnetic coordinates and magnetic midnight at FSMI are, respectively, 60.0° N, 248.1° E, 67.3°, 307.1°, and 8:05 UT. Panels (b) and (c) show the relative intensity of the luminosity at the lines of ~ 70.0° magnetic latitude (MLAT) and ~ 68.2° MLAT, respectively. Lower panels (d) and (e) show the magnetic and electric field variations with a bandpass filter of 60–600 s observed onboard TH-A. As can be seen from the keogram, Pc5 PMAA pulsations were often observed in association with the enhancement of the magnetic and electric field oscillations, for example, at ~ 1015–1050 UT, ~ 1105–1125 UT, ~ 1135–1200 UT, 1215–1240 UT, and ~ 1245–1300 UT. In this study, we focused on the time interval of 1210–1240 UT where the most outstanding Pc5 PMAA pulsations were observed, and the footprints of the THEMIS satellites were located in the fields of view of the FSMI all-sky imager, as shown below.

"Figure 2" shows the optical characteristics of the Pc5 PMMA pulsations observed at Fort Smith (FSMI) and Fort Simpson (FSIM) in Canada and the magnetogram observed at Yellowknife (YKNF) and FSIM. The magnetogram at FSMI was out of data during the event. The geographic and geomagnetic coordinates and magnetic midnight at FSIM are, respectively, 61.8° N, 238.8° E, 67.2°, 294.4°, and 8:55 UT; those at YKNF are, respectively, 62.5° N, 245.7° E, 69.3°, 302.7°, and 8:22 UT. It is found from the keogram at FSMI (upper panel) that the Pc5 PMMA pulsations occurred from ~ 1221 UT and, following, there were a clear three-cycle oscillations with a period of approximately 4.5 min, increasing their luminosity with time. The keogram observed at FSIM (panel (b) of “Figure 2”) also shows the Pc5 PMMA pulsations with three-cycles oscillations, but their luminosity decreased with time. The main occurrence region drifted equatorward with time during the three cycle oscillations. As can be seen from the combined all-sky snapshot images at both observatories (right panel), which show the spatial structure of the auroral forms giving rise to the keogram behavior, the auroral arc elongated approximately along the east-west direction from horizon to horizon, for more than 2000 km, though inclined slightly towards north-south. The north-south width of the auroral arc was narrow; it could be less than 20 km at the zenith of FSIM. FSIM is located at almost the same geomagnetic latitude as FSMI. When the event occurred at 1220 UT, the magnetic local time at FSMI and FSIM were 0325 MLT and 0235 MLT, respectively. Therefore, the auroral arc observed at FSIM appeared at a lower latitude than that at FSMI, which may indicate that the arc appeared approximately along the auroral oval, as the averaged auroral oval is located at the lowest latitude in the midnight region. YKNF is located approximately 2° higher in MLAT and 5° westward in MLON from FSMI. The Pc5 PMAA pulsations were observed over the zenith of YKNF using keogram and ASI. The magnetogram located at YKNF, to which a bandpass filter of 60–600 s was applied, demonstrated that an increase in the H-component started at ~ 1214 UT and reached its maximum amplitude at ~ 1218 UT. Subsequently, it decreased and reached its negative peak at ~ 1222 UT, which was followed by weak two-cycle oscillations with positive peaks at ~ 1225 UT and ~ 1229 UT. The oscillation amplitude of the H component was much larger than that of the D and Z components. Specifically, the maximum peak-to-peak (pp) amplitude of the H component was ~ 80 nT. The first negative peak at ~ 1222 UT indicated by the dotted line coincides with the occurrence of the first PMAA observed at FSMI. However, it is difficult to find clear coincidence with the H component of magnetic oscillations at the two subsequent PMAAs, especially at the third PMAA.

The magnetogram at FSIM shown in the panel (d) of "Figure 2", which is located at a lower latitude than YKNF, reveals almost the same signature of the magnetic pulsation as that seen at YKNF, although the amplitude of the magnetic pulsation is smaller than that observed at YKNF. For the relationship to the PMAA pulsations observed at FSIM, the magnetogram also revealed a similar signature as that seen at YKNF and FSMI.

Herein, we examine the characteristics of the Pc5 PMAA in detail. The top panel of "Figure 3a" repeats the keogram observed at FSMI. Hereinafter, we refer to the three sequences of PMAA as PMAA-1, PMAA-2, and PMAA-3. The bottom panel of "Figure 3a" depicts the expanded keogram of PMAA-2 in both the time and latitude at the dotted square, as marked in the top panel. "Figure 3b" shows the luminosity distribution over magnetic latitude for the time intervals (a), (b), and (c), which are depicted by vertical

lines in the bottom panel of "Figure 3a" during the PMAA-2. The time intervals (a), (b), and (c) correspond to the growing, maximum, and declining phases of the activity of PMAA-2, respectively.

We define a half-width of luminosity as $W(half) = W((I_p+I_g)/2)$, where I_p is the peak luminosity and I_g is the background luminosity. *W(half)* corresponds to the latitudinal width where the luminosity reduces to half of the peak luminosity. In the case of (b), I_p is ~ 6000 and I_g is ~ 4200; so, $(I_p+I_g)/2$ = ~ 5100. *W(half)* becomes ~ 0.6°. It is found that the *W(half)* was approximately the same at (a), (b), and (c). That is, the half-width of luminosity did not depend on the growing, maximum, and declining phases.

The upper panel of "Figure 4" shows the latitudinal distribution of the maximum auroral luminosity at each sampling time on the keogram for PMAA-1, PMAA-2, and PMAA-3. That is, each figure shows the maximum luminosity of aurora considering its latitude during the one-cycle of PMAA. It was found that the luminosity at PMAA-1 during the growing and maximum phases was lower than that at PMAA-2 and 3. Moreover, the luminosity at PMAA-2 was higher during the maximum and declining phases than that at PMAA-1 and 3 Furthermore, it was found that the luminosity at PMAA-3 was somewhat equal to that at PMAA-2 during the growing phase until ~ 69.1°, after which it formed a broad peak at approximately 69.1°- 69.4°. After the peak, the luminosity dropped sharply during the declining phase from ~ 69.4°. This demonstrates that the main region of PMAA-3 drifted further to the lower latitude side than that of PMAA-1 and PMAA-2. The latitude of the luminosity maximum during one cycle may correspond to the central region on the FLRs. The signatures shown above demonstrate the dynamic overall activity of PMAA during this event.

The lower panel of "Figure 4" shows the relative phase on the luminosity oscillation of PMAA versus magnetic latitude. In this figure, phase "zero" is the latitude where the luminosity was maximum in PMAA-2, at ~ 69.4° MLAT. The rate of the latitudinal phase variation was found to be ~ 75°/deg. This phase-latitude diagram demonstrates that the PMAA pulsations could be explained by the FLR model as demonstrated by previous studies, for example, Milan et al. (2001) and Samson et al. (2003), wherein it is demonstrated that this rate is ~ 165°/deg and 110°/deg, respectively.

To examine the PMAA feature in relation to the FLR model, it may be important to investigate a latitudinal dependency of the repetition period of PMAA pulsations between PMAA-1, PMAA-2, and PMAA-3. "Figure 5" depicts the luminosity plots with time for 10 luminosity lines, including line-190 (~ 68.7° MLAT) to line-223 (~ 70.5° MLAT). To visualize the periodicity at each line more easily, the plots were arranged as follows: the timing of the luminosity maximum at each line during the PMAA-1 was fixed at the same moment by shifting the start time. From this figure, the periodicity between PMAA-1 and PMAA-2 and that between PMAA-2 and PMAA-3 at each line can be easily found. An interesting feature is that the period between PMAA-1 and PMAA-2 on the lower latitude side between the line-190 (~ 68.7° MLAT) and line-218 (~ 70.0° MLA) was almost constant giving a period of ~ 265 s. On the other hand, the period at the higher latitude side between the line-218 and line-223 (~ 70.5° MLAT) increased from ~ 265 s to ~ 285 s. Moreover, during the interval between PMAA-2 and PMAA-3, the period on the lower latitude side between the line-190 and line-218 was constant, ~ 300 sec, whereas on the higher latitude side, it is difficult to find

a periodicity because no luminosity peak exists during the PMAA-3. Such a characteristic of low latitude portion as the constant period without latitudinal dependence, e. g., monochromatic oscillation, fits to the FLR model proposed by Chen and Hasegawa (1974) and Southwood (1974), though the period between PMAA-2 and 3 is longer than that between PMAA-1 and 2. On the other hand, the period at higher latitude side of PMAA, between PMAA-1 and 2, lengthens with increasing latitude. This characteristic suggests that the period is related to the local filed line length.

3-2-2. Field-line resonance signals observed in space

"Figure 6" shows auroral snapshot images observed at FSMI during the time period from the growing phase of the auroral arc pulsation at (a) 1226:00 UT to the declining phase at (c) 1228:09 UT thorough the maximum phase at (b) 1226:57 UT plotted with the footprints of TH-A, TH-D, and TH-E spacecraft at a 110 km altitude based on the TS05 model. The footprints were calculated by the TS05 model using following parameters: Dst, -28.0 nT; solar wind dynamic pressure, 2.0 nPa; interplanetary magnetic field (IMF) By, 0.5 nT; and Bz, as -1.5 nT. In each snapshot image, the footprints were shown with the triangle symbol under the half-hour trajectory during 1210–1240 UT (see the spatially expanded plot in "Figure 6"). Although TH-D was located in the most westward side and TH-A was located at the highest latitude side, the footprints of the three satellites were located very close to each other, as shown in the plot figures of "Figure 6". The model-calculated footprint was well within the fields of view of the ASIs where the auroral arc was detected, and the footprints were located on the poleward side from the PMAA during most of time in this study. The snapshot image at 1226:00 UT ((a) in "Figure 6") demonstrates that the auroral arc with higher luminosity at the eastern part was located a few tens of kilometers poleward from the zenith. At 1226:57 UT ((b) in "Figure 6"), the luminosity enhancement region elongated westward and moved in the poleward direction. Hence, the footprints of the spacecraft were located more equatorward relative to (a). At 1228:09 UT ((c) in "Figure 6"), the portion of the auroral arc moved more poleward with decreasing luminosity, so the footprints of the spacecraft were located more equatorward than in (a) and (b), and were located at just poleward boundary of the PMAA. A faint PMAA-3 appeared at the lower latitude side of the PMAA-2.

"Figure 7" shows the spacecraft orbit configuration projected onto three different planes (X-Y, X-Z, and Y-Z) in the geocentric solar magnetospheric (GSM) coordinate system during 1210–1240 UT on 2nd March 2011. The details of the orbit of TH-A, TH-D, and TH-E at 1210 UT on the X, Y, and Z planes with GSM coordinates are the following: X is ~ -6.2 Re, ~ -6.0 Re, and ~ -6.0 Re; Y is ~ -9.8 Re, ~ -9.5 Re, and ~ -9.8 Re; and Z is ~ 1.4 Re, ~ 1.0 Re, and ~ 1.0 Re. These orbits demonstrate that, at ~ 0410 MLT, the spacecraft were located near the northern hemisphere' s magnetic equatorial region in the post-midnight sector. Regarding the relative orbital location among the three satellites, it is worth noting that TH-D was located at almost the same position as TH-E in the X and Z coordinates, but they were separated by ~ 0.2 Re in the Y direction, and the position of TH-A was located at almost the same position as TH-E in the Y plane, but was separated by 0.4 Re northward in the Z plane from TH-D and TH-E.

In the following analysis, general mean-field-aligned (MFA) coordinates were used. In this system, the Z component is parallel to the average direction of the ambient magnetic field, the Y component is azimuthally perpendicular to the magnetic meridian (westward), and the X component is roughly in the radial direction. Since the magnetic field near the equatorial plane was stretched, deviating from a dipole-like topology. We found that, when the data were plotted on GSM coordinates, the X and Y components of the magnetic field intensity were comparable to the total magnetic field intensity (not shown here the figure). This signal suggests that the field-line topology was extremely stretched to tail-ward. Therefore, the MFA coordinate system can display more physically understandable wave signals than the GSM coordinate system. The average magnetic field was calculated as sliding averages of 600 points (30 min) of observed magnetic field variations.

The panel (a) of "Figure 8" depicts auroral keogram observed at FSMI. The vertical dotted line at ~ 1221 UT indicates the start time of the luminosity enhancement of the PMAA. The panel (b) of "Figure 8" demonstrates the intensity of the luminosity at line ~ 70.2° MLAT near the footprint location of TH-D and TH-E, as presented later in **Table-1**, with a lowpass filter of 60 s. The panel (c) of "Figure 8" graphs the X component of the electric field (Ex) displayed with a lowpass filter of 60 s. The positive oscillation started at ~ 1218 UT, as indicated by a vertical solid line, simultaneously onboard the TH-A, TH-D, and TH-E spacecraft. It was found that the oscillation of the Ex started ~ 3 minutes earlier than that of the luminosity enhancement of the Pc5 PMAA. Subsequently, the signal displayed three-cycle oscillations and a weak increase at the fourth cycle oscillation, which could correspond to the fourth cycle oscillation with weak luminosity, as shown in the panel (a) of "Figure 8". Furthermore, it was observed that the oscillation amplitude attained a maximum at the second cycle, which may correspond to the occurrence of PMAA-2, whose luminosity was highest among three cycles of PMAA, as demonstrated in "Figure 4". It was noticed that after the start of the oscillation at ~ 1218 UT, the oscillation at TH-A exhibited a phase lag with respect to that of TH-D and TH-E. Moreover, this relative phase lag between TH-A and TH-D lengthened during the following oscillations. This implies that the period of the Ex oscillation in TH-A was longer than that in TH-D and TH-E. Such signatures are more clearly found in the Y component of magnetic field (By) variations as seen in the panel (d) of "Figure 8" This signature is the same as the periodicity of PMAA observed at the higher latitude side (~ 70.0°-70.5° MLAT), as depicted in "Figure 5" where the period between PMAA-1 and PMAA-2 lengthened with increasing latitude. This signature suggests that the footprint of TH-A could be located in the region of the higher latitude side of the PMAA. Accordingly, this characteristic suggests that the period relates to the local filed line length. The oscillation phase lag at the field line of the poleward location suggests that these waves were generated by FLR. However, the FLR model (Chen and Hasegawa, 1974; Southwood, 1974) postulates that waves are monochromatic, that is, the wave period is the same everywhere, as demonstrated in "Figure 5." Therefore, the features observed at TH-A did not agree with the monochromatic frequency FLR model, instead they indicated that each field line oscillates at a different eigen-frequency. This is discussed further in **Session 4.** Furthermore, before the oscillations started, the base-line intensities at TH-A, TH-D, and TH-E were ~ − 6 mV/m, − 9 mV/m, and − 3 mV/m, respectively. The peak-to-peak amplitudes of TH-D and TH-E were almost the same during the entire oscillation period, whereas the amplitude at TH-A was ~

20–30% larger than that at TH-D and TH-E during the first cycle, and became comparable to that at TH-D and TH-E during the second and third cycles. It is worth noting that the relative intensity difference between TH-D and TH-E was rather high in comparison to the By as seen in the panel (d) of "Figure 8". It was found that the oscillation amplitude at TH-A was larger than that at TH-D and TH-E, whereas the amplitudes of TH-D and TH-E were approximately equal. Moreover, the oscillation amplitude attained a maximum at the second cycle, which may correspond to the PMAA-2, in the same manner as demonstrated in the Ex behavior. The fundamental-mode Alfven waves have the property that the magnetic node is located at the equatorial region; therefore, it is reasonable that the amplitude at TH-A was larger than at TH-D and TH-E, because TH-A was located at ~ + 1.4 Re in the Z coordinate and TH-D and TH-E were located more equatorward at ~ + 1.0 Re in the Z coordinate, as shown in "Figure 7." It was also observed that the oscillation of TH-A exhibited a phase lag with respect to that of TH-D and TH-E. The TH-A lag time from TH-E at the positive first, second, third, and fourth peaks were ~ 20 s, ~ 30 s, ~ 80 s, and ~ 90 s, respectively. Moreover, the relative phase lag between TH-D and TH-E was less than ~ 20 s in all four peaks.

The compressional mode wave at the Z component of magnetic filed (Bz) oscillations is plotted in the panel (e) of "Figure 8." This field-aligned component of the magnetic field demonstrated that both the baseline and oscillation amplitude were larger at TH-A than at TH-D and TH-E. The relative amplitudes at TH-D and TH-E were approximately equal. Such characteristics are reasonably explained by the relative location of the spacecraft. That is, TH-A was located at the higher latitude side (in the northern hemisphere) from the magnetic equator, than TH-D and TH-E. Furthermore, TH-A data demonstrated that a negative oscillation started from ~ 1218 UT and reached a negative peak at ~ 1220 UT, after which it formed a positive peak at ~ 1222 UT, whereas TH-D and TH-E presented weaker negative and positive peaks almost simultaneously with TH-A. Subsequently, the waveforms at TH-A displayed a phase lag from TH-D and TH-E signals in the same manner as documented above.

The panel (f) of "Figure 8" presents the variation in ion pressure based on Electrostatic Analyzer observation made by three satellites. It was found that the pressure was gradually increased with time until ~ 1218 UT at the location of all three satellites, after which the pressure decreased with time and started the long-period oscillations. The pressure at TH-E was higher than that at TH-D and TH-A during the entire event. This suggests that TH-E would be located closer to the central plasma sheet than the TH-D and TH-A because the ion pressure escalates at that location. It is interesting to note that the decrease in ion pressure started at ~ 1218 UT, which is when the Ex and By oscillations started. The luminosity peaks, which are marked with vertical long and short dash lines in the panel (b) of "Figure 8", correspond to the pressure peaks observed at TH-D and TH-E.

To compare the magnetic field pulsations observed on the ground and in the magnetosphere, the H component of the magnetogram observed at YKNF is repeated in the panel (g) of "Figure 8" with a band pass filter of 60–600 s. It can be seen that the H component of the magnetic field increased with time until ~ 1218.30 UT, after which it decreased with time until ~ 1222.00 UT. It is important to note that the signature of the magnetic variations observed on the ground does not indicate a clear correlation with

that observed on the magnetospheric By magnetic oscillations, as shown in the panel (d) of "Figure 8". On the other hand, the signatures observed on the ground magnetometer demonstrate a rather similar behavior to that observed in case of ion pressure variation in the magnetosphere as shown in the panel (f) of "Figure 8", especially during the interval of ~ 1214–1226 U.

3-2-3. Cross-correlation analysis between FLR oscillations and optical luminosity pulsations

To examine the relationship between the magnetic and electric field oscillations in the magnetosphere and the optical luminosity pulsations observed on the ground, we performed a cross-correlation analysis among the luminosity lines of 223, 220, 210, and 200, which correspond to the MLAT of ~ 70.5°, ~ 70.2°, ~ 69.5°, and ~ 69.0°, and the magnetic field and electric field variations observed onboard the TH-A, TH-D, and TH-E spacecraft with a bandpass filter of 60–600 s.

"Figure 9" shows an example of the result of the cross-correlation analysis. The left two panels show the power spectra of the By oscillations at TH-D (upper panel) and the luminosity pulsations at line 220 (lower panel). Meanwhile, the right two panels of "Figure 9" show the coherence (upper panel) and the phase difference (lower panel) between the two data. It can be seen that the coherence had a high value of more than 0.9 at the period of ~ 200–300 s, and the phase difference was ~ 150°. The power spectrum did not show a clear peak power at the specified period in this cross-correlation analysis.

"**Table 1**" shows the summary of the coherence around the period of ~ 200–300 s between the luminosity pulsations at lines 223, 220, 210, and 200 observed on the ground, and the X, Y, and Z components of the magnetic and the X and Y components of the electric field oscillations observed onboard the TH-A, TH-D, and TH-E satellites. Higher coherence columns, > 0.8 are shown in different colors. From this, the magnetic field (Bx, By, Bz) and electric field (Ex, Ey) variations and the luminosity pulsation at line 220 showed the highest correlation when compared with the other luminosity lines for the TH-D and E satellites, and that at line 223 for the TH-A. Meanwhile, the coherence with the luminosity at line 200 had the lowest value for the TH-A, D, and E satellites. From these results, we can draw an important conclusion that the luminosity pulsations around line 220 and 223 correlated well with the magnetic and electric oscillations observed in the magnetosphere. This indicates that the real footprints of the TH-A, TH-D, and TH-E satellites may be located near the field line of lines 223 and 220. Moreover, the footprints calculated by the TS05 model shown in "Figure 6" were located at the poleward side on the PMAA, which showed good agreement with the results shown in "**Table 1**". For the relation between the Z component of the magnetic field (Bz) variations and the luminosity pulsations, a high coherence (> 0.9) was found to occur at lines 220 and 223.

The detailed comparison of the periods of the Pc5 PMAA pulsations and the magnetospheric magnetic and electric field oscillations is very interesting and important. The panel (a) of "Figure 10" shows the auroral keogram observed at FSMI. The panel (b) of "Figure 10" shows the relative luminosity of the auroral keogram at line 210 (~ 69.5° MLAT) (green), 215 (~ 69.8° MLAT) (black), and 220 (~ 70.2° MLAT) (light blue) with a low pass filter of 30 s. The time at each positive peak was delayed at the higher latitude lines (poleward moving signal). Furthermore, the periods between the first and second peaks at lines 210,

215, and 220 were estimated to be ~ 265 s, ~ 265 s, and ~ 275 s, respectively. The periods between the second and third peaks at lines 210 and 215 were ~ 300 s and ~ 293 s. The lines 210 and 215 are located in the monochromatic frequency FLR region where the period is constant and independent of latitude. Moreover, line 220 is located in the multi-frequency FLR region where the period dilates with increasing latitude, as plotted in "Figure 5." The panel (c) of "Figure 10" shows the Y component of the magnetic field observed at TH-A, TH-D, and TH-E. The periods at TH-D and TH-E are approximately equal, whereas the period at TH-A is longer than that at TH-D and TH-E. This signature suggests that the TH-D and TH-E were located in the monochromatic frequency FLR region, but the TH-A was located at a multi-frequency FLR region. It is worth noting that the repetition period of the magnetic oscillation was ~ 10–25% longer than that of the Pc5 PMAA pulsations.

3–3. Relation between FLR and Solar wind parameters

The source mechanism of the FLR that has received the most attention is surface instabilities at the magnetopause (such as Kelvin–Helmholtz instability (KHI) and pressure impulse in the solar wind plasma) [Rostoker and Sullivan, 1987; Engebretson et al., 1998; Kivelson and Southwood,1985]. If the ground-based Pc5 PMAA pulsations are the result of this instability, it is likely that their characteristics depend on solar wind conditions. Therefore, we now examine this relationship. The panels (a) and (b) of "Figure 13" show the Y component of the magnetic field and the Y component of flow velocity, respectively, observed onboard the TH-A. The panels (c) and (d) of "Figure 11" show the Y and Z components, respectively, of interplanetary magnetic field (IMF), the panels (e) and (f) of "Figure 11" show the solar wind flow speed and pressure, and the panel (g) of "Figure 11" shows the AE index. The solar wind and IMF parameters were taken from the time-shifted OMNI-1 min data. The highlighted region indicates the time interval we examined. It is found from (a) and (b) that few FLR cycle signals were sporadically observed before and after our observations. Corresponding to these FLR oscillations, the Pc5 PMAA pulsations were also observed on the ground as shown in "Figure 1". By looking at IMF Bz, it is found that the FLR phenomena in this study were observed during the period of positive Bz after a recovery of about 1.5 hours of negative Bz, which started at ~ 1045 UT. It is worth noting that a positive Bz (~ 2 nT) was observed at ~ 1220 UT when the FLR phenomena were observed. The most distinct characteristic is that the solar wind speed was very high, approximately 650 km/s, during the observations. We will take a look on solar wind conditions in more detail for this event using Geotail data.

Geotail satellite was located at the upstream region near the dayside magnetopause. The orbit at 1200 UT on the X, Y, and Z planes with GSM coordinates was 19.6 Re, ~ -22.0 Re, and ~ -6.1 Re. The panel (a) of "Figure 12" shows the X, Y, and Z components of the magnetic field observed at TH-A. The Pc5 oscillations were observed from ~ 1218 UT at the vertical line in this figure, as shown in "Figure 8." The IMF magnetic field and the solar wind speed data obtained by Geotail was significantly different from the data obtained from OMNI, as depicted in "Figure 11". Sudden changes were observed at ~ 1219 UT on IMF By (from ~ -3 nT to ~ 2 nT) and Bz (from ~ 2 nT to ~ -2 nT). Similar sudden changes were also found in the solar wind velocity at Vy (from ~ 20 km/s to ~ 50 km/s) and Vz (from ~ 30 km/s to ~ -10 km/s). Even if we assumed that these drastic changes in the IMF and solar wind speed could trigger the FLR

oscillations, their timing would be inconsistent. Specifically, because the Vx is ~ 660 km/s, it takes approximately 4–5 minutes when the rapid change of the solar wind observed at Geotail reaches TH-A. Therefore, under the general/standard solar wind condition, we have to exclude the possibility that the magnetospheric magnetic and electric field oscillations observed at ~ 1218 UT onboard TH-A were affected by the solar wind discontinuity observed at 1219 UT onboard Geotail. However, when we checked the polar cap Super Dual Auroral Radar Network (SuperDARN) (Greenwald et al., 1995;

Chisham et al., 2007; Nishitani et al., 2019) data for the scan plots of the line of site velocity obtained at Rankin Inlet (Geo. lat. 62.8°, lon. − 92.1°; Mag. lat. 71.5°, lon. − 21.7°), as depicted in the panel (a) and the map potential plot data in the panel (b) of "Figure 13," we found that the polar cap convection enhanced to more than ~ 800 m/s from ~ 1218 UT. These signatures obtained from the SuperDARN data indicate a typical convection pattern under the sudden negative changes in IMF Bz (Ruohoniemi and Greenwald, 1998; Shepherd et al., 1999). To explain why the discontinuity arrived at Earth's magnetopause earlier than Geotail, we can speculate that the surface discontinuity of the solar wind had large tilt in the Vx direction. Under this condition, the sudden negative changes in the IMF Bz may cause the sudden enhancement of magnetospheric convection, which could have affected the generation of the FLR oscillations, and caused the thinning of plasma sheet, as shown in "Figure 8." The negative Bz also caused the expansion of the auroral oval, after which, the primary occurrence region of PMAA drifted equatorward with time, as shown in "Figures 2, 4, and 8."

4. Discussion

In this study, we reported on the observational evidence of the Pc5 PMAA, magnetic pulsations, and the magnetospheric magnetic and electric field oscillations through the ground-space coordinated observations.

We examined Pc5 magnetic pulsations from the ground at YKNF (69.3° MLAT, 302.7° MLON) and FSIM (67.2° MLAT, 294.4° MLON), as depicted in "Figure 2." The oscillation signatures observed at the two observatories were somewhat similar, although the amplitude of the magnetic pulsation at YKNF, where the PMAA pulsations were observed over the zenith of the observatory, was larger than that at FSIM. Moreover, the H component of magnetic variations observed at the two observatories did not exhibit a clear coincidence with the PMAA pulsations. Previous studies reported that the Pc5 magnetic pulsations and auroral luminosity pulsations showed good correlation, and that both pulsations have a latitudinal phase shift variation (e.g., Xu, et al., 1993; Milan, et al., 2001; Samson et al., 1996, 2003). On the other hand, this event showed that the magnetic variation on the ground neither exhibited a clear coincidence with the PMAA pulsations, nor with magnetospheric magnetic By oscillations, as demonstrated in "Figure 8." These signatures suggest that the magnetic pulsations observed on the ground could not correspond directly to the PMAA pulsations. Furthermore, it was found that the H component of magnetic pulsations observed on the ground demonstrated a rather similar behavior to that of the ion pressure variation in the magnetosphere. As examined above, the magnetic pulsations observed on the ground exhibited complex signatures that were not well correlated with the PMAA, and so far we do not have a clear explanation for

the apparent correlation between the ground magnetic field and the magnetospheric pressure. Clarifying the physical relationship between these variations requires further work.

As demonstrated in "Figure 5," the periodicity of the Pc5 PMAA pulsations presented an intriguing signature. The recurrence periods on the lower latitude region (~ 68.5°-70.0° MLAT) between PMAA-1 and 2, and PMAA-2 and 3 were almost constant ~ 265 s and ~ 300 s. These signatures demonstrate that the lower latitudinal region of the PMAA pulsations conformed to the monochromatic frequency FLR region, where the period is constant and without latitudinal dependence. Such a monochromatic FLR model was proposed by Chen and Hasegawa (1974) and Southwood (1974). The phase-latitude profiles of the PMAA pulsations at the lower latitude region (~ 68.5°-70.0° MLAT), as shown in "Figure 4," also demonstrated that these signatures fitted to the monochromatic frequency FLR model, as reported by Milan et al, (2011) and Samson et al., (2003). However, the period increased from ~ 265 s (between PMAA-1 and 2) to ~ 300 s (between PMAA-2 and 3). It is suggested that the FLR condition, such as field-line length and/or plasma density, could change during the time interval. On the other hand, in the higher latitude region (~ 70.0°-70.5° MLAT), the period lengthened with increasing latitude, which indicates that the higher latitude side of the PMAA exhibits a multi-frequency FLR region and that the period was proportional to the local field line length. It means that the two different types of FLR oscillations were excited simultaneously. To the best of our knowledge, there are no reports of such FLRs observations.

From the luminosity distribution analysis as graphed in "Figure 3b," the latitudinal half-width of the arc luminosity was ~ 0.6°. It was also found that its size was somewhat constant during the enhancement of PMAA from the growing phase to the declining phase. It is widely known that the auroral arc luminosity is proportional to the intensity of field-aligned current (FAC) (e.g., Borovsky, 1993). If a half-width of luminosity corresponds to the latitudinal width of the FAC, the features mentioned above suggest that the width of FAC was invariable from growth to the declining phase of PMAA. The latitudinal width of the FAC was ~ 0.6 degree at that moment. The FAC region moved poleward in association with the movement of PMAA within the latitude from ~ 68.5° to ~ 70.5° MLAT. The generation of PMAA may closely relate to FLR; therefore, the location of the luminosity maximum during one cycle of PMAA may correspond to the central resonance region of the FLR, where the field of the line matches the resonance frequency.

In the following, we discuss the influence of the magnetospheric magnetic and electric field oscillations observed at the THEMIS spacecraft on the Pc5 PMAA pulsations in the ionosphere and the magnetosphere-ionosphere (M-I) coupling processes to connect both.

Using the data of THEMIS ground-space coordinated observations, we found that the Pc5 PMAA pulsations observed on the ground occurred in conjunction with the enhancement of the magnetic and electric field oscillations observed near the equatorial plane of the magnetosphere. The magnetic and electric field signal displayed three-cycle oscillations and a weak increase at the fourth cycle oscillation, similar to the main PMAA pulsations and the fourth cycle oscillation with weak luminosity. It is found the oscillation amplitude showed a maximum at the second cycle that corresponded to the occurrence of the

PMAA-2 whose luminosity was highest among the three-cycle main pulsations. It was also found that the coherence between the magnetic and electric field oscillations and the luminosity pulsations had a high value of more than 0.9. From these observations, **it is suggested** that the PMAA pulsations and the magnetospheric field oscillations were initiated by the same physical mechanism (presumably originating in the magnetospheric side) and thus they oscillated concurrently through the M-I coupling. These results are consistent with previous reports (e.g., Xu, et al., 1993; Samson et al., 1996, 2003; Milan et al., 2001), which mainly obtained ground-based network observations.

The PMAA signal showed that the arc elongates a few thousand kilometers in the east-west direction, but only a few tens of kilometers in the north-south direction. Such features are similar to those of a stable discrete auroral arc that is commonly observed in the evening sector (Gillies et al., 2014). These signals suggest that both the discrete stable arc and the PMAA were generated by a similar mechanism. The generation mechanism of a stable discrete auroral arc is thought to be associated with the upward field-aligned electric field, which accelerates auroral electrons and enhances the auroral luminosity.

Many experimental and theoretical studies have focused on investigating the mechanism that produces such a field-aligned electric field. Examples include static magnetosphere-ionosphere couplings, mirroring of electrons, electrostatic double layers, and dispersion in kinetic or electron inertia Alfven waves in the auroral acceleration region at ~ 1–2 RE (see the review by Borovsky, 1993). However, such physical processes are still under discussion. If we apply a field-aligned electric field model to the generation mechanism in this study, the Pc5 PMAA pulsations could be associated with the field-aligned electric field that could be caused by the magnetospheric magnetic and electric field oscillation.

It was found that the compressional component of the magnetic field (Bz) oscillations displayed high coherence with the luminosity pulsations as shown in "Figure 8" and "**Table 1**". It is known that the long period modulation of diffuse patch aurora/pulsating aurora is thought to be caused by the electron pitch-angle scattering with compressional mode Pc5 pulsations (Oguti et al., 1987; Yamamoto, 1988; Saka et al., 2014). To the best of our knowledge, reports concerning compressional magnetic pulsations causing a discrete auroral arc are somewhat limited to sudden commencement (SC) related auroral events (e.g., Liu et al., 2011; 2013). The contribution of the compressional magnetic pulsation to the Pc5 PMAA pulsation is intriguing; however, it requires further study.

Our study may offer important observational results to investigate the mechanism of producing a field-aligned electric field from the magnetic and electric field oscillation, particularly the magnetosphere-ionosphere (M-I) coupling processes. The relationships between the field-aligned electric fields in the electron acceleration region at an altitude of ~ 1–2 RE and the magnetic and electric field oscillations near the equatorial plane in the magnetosphere are essential to consider the generation of this phenomena. To investigate this relationship in future works, coordinated observations are necessary for simultaneous observations of the magnetic and electric field waves near the equatorial plane, the field-aligned current and the precipitating electron flux in the ionosphere, and the optical PMAA pulsations, as well as a numerical simulation study.

In previous studies, three-generation mechanisms of the FLR oscillations have been postulated. The first is a KHI caused by the velocity shear between the solar wind and the magnetopause (Southwood, 1974; Chen and Hasegawa, 1974), the second is the pressure impulse/oscillation in the solar wind plasma (Kivelson and Southwood,1985), and the third is the Alfven impulse caused by the sudden magnetospheric convection changes by the sudden IMF Bz changes (Kozlovsky and Kangas, 2002). In "Figures 11 and 12", we showed that the solar wind speed was very high, approximately 650 km/s, during the event on the 2nd March 2011. This suggests that the KHI could be the most likely cause of the FLR.

On the other hand, it was found from the panel (c) and (d) of "Figure 8" that the electric and magnetic field oscillations on the three satellites started simultaneously with synchronized waveforms, and subsequently, the waveform at the TH-A (located at higher latitudes) displayed a phase lag relative to those at TH-D and TH-E. The oscillation period of the magnetic and electric field at higher latitudes was longer than that at lower latitudes, which demonstrates the oscillations of individual magnetic shells. This suggests that the field line oscillations were triggered simultaneously in a wide region by an impulse, such as rapid convection changes caused by the sudden variations of the IMF Bz observed by SuperDARN radar and Geotail satellite, as shown in "Figures 12 and 13". Further observations are required to understand their generation mechanism.

5. Summary

This study constitutes the first coordinated observation of the Pc5 PMAA pulsations (~ 4–5 min in period) and magnetic pulsations on the ground and the magnetic and electric field oscillations onboard THEMIS spacecraft near the equatorial plane of the magnetosphere, whose footprints were located near the Pc5 PMAA pulsations in the post-midnight sector.

The optical characteristics of the Pc5 PMMA pulsations demonstrated that the east-west aligned arcs, more than 2000 km long, moved poleward with clear three-cycle oscillations within a period of ~ 4.5 min. The north-south width of the arc was narrow, less than 20 km, at the minimum scale.

The Pc5 magnetic pulsations were observed in association with the Pc5 PMAA pulsations. The amplitude of the H component was much larger than that of the D and Z components. The magnetic variations on the ground exhibited a clear coincidence neither with the PMAA pulsations, nor with the magnetospheric magnetic field oscillations. On the other hand, variations in the H component of magnetic pulsations demonstrated a rather similar behavior to that of the ion pressure variation within the magnetosphere.

The characteristics of the Pc5 PMAA demonstrated that the latitudinal half-width of the arc luminosity was ~ 0.6 degree and its size was approximately unchanged during the enhancement of PMAA from its growing phase to its declining phase. This scale may represent the latitudinal width of the field-aligned current region at that moment.

It is found that the recurrence period of the PMAA pulsations was almost constant in the lower latitude region (~ 68.5°-70.0° MLAT). On the other hand, the period at higher latitude region (~ 70.0°-70.5° MLAT)

lengthened. This signature demonstrated that the oscillations on the lower latitudinal side of the PMAA conformed with the monochromatic frequency FLR region, where the period is the constant and without latitudinal dependence. Such a monochromatic FLR model was proposed by Chen and Hasegawa (1974) and Southwood (1974). Meanwhile, the higher latitude side of the PMAA presented a multi-frequency FLR region where the period increased with increasing latitude. The phase-latitude profile of the PMAA pulsations on the lower latitude region also demonstrated that these signatures fitted with the monochromatic frequency FLR model.

Pc5 PMAA pulsations occurred in conjunction with the enhancement of the magnetic and electric field oscillations in the magnetosphere. This magnetospheric oscillation signal displayed three-cycle oscillations and a weak increase at the fourth cycle oscillation, which corresponded to the main PMAA pulsations and the fourth cycle oscillation with weak luminosity, respectively. It was also found from the cross-correlation analysis that the coherence between the magnetospheric magnetic and electric field oscillations and the luminosity pulsations had a high value of more than 0.9. From these observations, it is suggested that the PMAA pulsations and the magnetospheric field oscillations were initiated by the same physical mechanism (presumably originating in the magnetospheric side), and thus, they oscillated concurrently through the M-I coupling.

The coordinated satellite data also indicated that the period of the magnetospheric magnetic and electric field oscillation was longer at the higher latitude site, thereby demonstrating a multi-frequency FLR region.

The solar wind speed was significantly high, approximately 650 km/s, during this event. The magnetospheric magnetic and electric field oscillations could be triggered simultaneously in a wide region by an impulse, such as rapid convection changes caused by the sudden variations of the IMF Bz observed by the SuperDARN radar and Geotail satellite.

Abbreviations

ASI: all-sky imager

ATHA: Athabasca

FAC: field-aligned current

FLR: field-line resonance

FSMI: Fort Smith

FSIM: Fort Simpson

FYKN: Fort Yukon

GBO: Ground-Based Observatory

IMF: interplanetary magnetic field

KHI: Kelvin–Helmholtz instability

MLAT: magnetic latitude

MLON: magnetic longitude

MLT: magnetic local time

PMAA: poleward moving auroral arc

SC: sudden commencement

THEMIS: Time History of Events and Macroscale Interactions during Substorm

SuperDARN: Super Dual Auroral Radar Network

YKNF: Yellowknife

Declarations

Availability of data and materials

The summary plot of the THEMIS data are available from the home page of < http://themis.ssl.berkeley.edu/summary.php?year=2019&month=03&day=05&hour=0024&sumType=tha&type=overview>, and THEMIS all-sky imager data are available from the < http://themis.ssl.berkeley.edu/gbo/display.py?date=2013.02.07&view_type=summary&submit=Start>. THEMIS Data Overview is from <http://themis.ssl.berkeley.edu/overview_data.shtml>. THEMIS data analyzing software is called SPEDAS, and is available from < http://themis.ssl.berkeley.edu/software.shtml>. Geotail data are available from the < https://www.darts.isas.jaxa.jp/stp/geotail/>. SuperDARN data are available from the < http://vt.superdarn.org/tiki-index.php?page=DaViT+Multi+Scan+Plot>.

Acknowledgements

This work was partially supported by the Inter-university Upper atmosphere Global Observation NETwork (IUGONET) project funded by the Ministry of Education, Culture, Sports, Science and Technology of Japan. Part of the work of TH has been done at ERG-Science Center (ERG-SC) operated by ISAS/JAXA and ISEE/Nagoya University. The authors acknowledge NASA contract NAS5-02099 for the use of data from the THEMIS Mission. Specifically, we thank S. Mende and E. Donovan for use of the ASI data. Deployment and data retrieval of the THEMIS ASIs was partly supported by CSA contract 9F007-046101. THEMIS all-sky image data are available through the open data repository at UC Berkeley at http://themis.ssl.berkeley.edu/index.shtml. Geotail magnetic field and plasma data were provided by S.

Kokubun, T. Nagai and Y. Saito through DARTS at Institute of Space and Astronautical Science, JAXA in Japan. We would also like to thank all of the Principal Investigators of the SuperDARN radars. We would like to thank Editage (www.editage.jp) for English language editing.

Authors' contributions

NS analyzed THEMIS data. TH and YT arranged data analysis software. AK and AY discussed about the ionospheric convection and field aligned current. All authors read and approved the final manuscript.

Funding

This work was supported by a Grant-in-Aid for Scientific Research from the Japan Society for the Promotion of Science, KAKENHI Grant Numbers 15K05305, 25287129, and 19K03949.

Ethics declarations

Ethics approval and consent to participate

Not applicable.

Concept for publication

Not applicable.

Competing interests

The authors declare that they have no competing interests.

References

1. Angelopoulos V (2008), The THEMIS mission, Space Sci. Rev., 141,5–34. doi:10.1007/s11214-008-9336-1.
2. Auster H, et al (2008), The THEMIS fluxgate magnetometer, Space Sci. Rev., 141, 235–264. doi:10.1007/s11214-008-9365-9.
3. Baker G, Donovan EF, and Jackel BJ (2003), A comprehensive survey of auroral latitude Pc5 pulsationcharacteristics, *J. Geophys. Res.*, 108, 1384–1397. doi:10.1029/2002JA009801.
4. Baddeley LJ, Lorentzen DA, Partamies N, Denig M, Pilipenko VA, Oksavik K, Chen X, and Zhang Y (2017), Equatorward propagating auroral arcs driven by ULF wave activity: Multipoint ground- and space-based observations in the dusk sector auroral oval, J. Geophys. Res. Space Physics, 122, 5591–5605. doi:10.1002/2016JA023427.
5. Bonnell JW, Mozer FS, Delory GT, Hull AJ, Ergun RE, Cully CM, Angelopoulos V, and Harvey PR (2008), The electric field instrument (EFI) for THEMIS, Space Sci. Rev., 141, 303–341. doi:10.1007/s11214-008-9469-2.

6. Borovsky JE (1993), Auroral arc thickness as predicted by various theories, J. Geophys. Res., 98, 6101.
7. Chen L, and Hasegawa A (1974), A theory of long-period magnetic pulsations: 1. Steady state excitation of field line resonance, J. Geophys. Res., 79, 1024–1032.
8. Chisham G, Lester M, Milan SE, Freeman MP, Bristow WA, Grocott A, McWilliams KA, Ruohoniemi JM, Yeoman TK, Dyson PL, Greenwald RA, Kikuchi T, Pinnock M, Rash JPS, Sato N, Sofko GJ, Villain J-P. and Walker ADM (2007), A decade of the Super Dual Auroral Radar Network (SuperDARN): scientific achievements, new techniques and future directions, Surv. Geophys., 28, 33. doi:10.1007/s10712-007-9017-8.
9. Engebretson M, Glassmeier K, Stellmacher M, Hughes WJ, and Luhr H (1998), The dependence of high latitude Pc5 wave power on solar wind velocity and on the phase of high speed solar wind streams, J. Geophys. Res., 103, 26,271.
10. Fenrich FR, Samson JC, Sofko G, and Greenwald RA (1995), ULF high- and low-m field line resonances observed with the Super Dual Auroral Radar Network, J. Geophys. Res., 100(A11), 21, 535-21 548. doi:10.1029/95JA02024.
11. Gillies DM, Knudsen DJ, Donovan EF, Spanswick EL, Hansen C, Keating D, & Erion S (2014), A survey of quiet auroral arc orientation and the effects of the interplanetary magnetic field. Journal of Geophysical Research: Space Physics, 119, 2550–2562. https://doi.org/10.1002/2013JA019469
12. Gillies DM, Knudsen D, Rankin R, Milan S, & Donovan E (2018), A statistical survey of the 630.0-nm optical signature of periodic auroral arcs resulting from magnetospheric field line resonances. Geophysical Research Letters, 45, 4648–4655. https://doi.org/10.1029/ 2018GL077491
13. Greenwald RA, Baker KB, Dudeney JD, Pinnock M, Jones TB, Thomas EC, Villain J-P, Cerisier CS, Hanuise C, Hunsucker RD, Sofko G, Koehler J, Nielsen E, Pellinen R, Walker ADM, Sato N, Yamagishi H (1995), DARN/SuperDARN: A global view of the dynamics of high-latitude convection, Space Sci. Rev., 71, 761-796, doi:10.1007/BF00751350.
14. Kivelson M and Southwood D (1986), Coupling of global magnetospheric MHD eigenmodes to field line resonances, J. Geophys. Res., 91, 4345– 4351.
15. Kokubun S (2013), ULF waves in the outer magnetosphere: Geotail observation 1 transverse waves, *Earth Planets Space*, 65, 411–433.
16. Kozlovsky A & Kangas J (2002), Motion and origin of noon high latitude poleward moving auroral arcs on closed magnetic field lines, J. Geophys. Res., 107(A2), 1017. doi:10.1029/2001JA900145.
17. Lessard M (2012), A review of pulsating aurora, in Auroral Phenomenology and Magnetospheric Processes: Earth and Other Planets, edited by A. Keiling et al., Geophys. Monogr. Ser., 197, 55–68. doi:10.1029/2011GM001187.
18. Liou K, Takahashi K, Newell PT, Yumoto K (2008), Polar Ultraviolet Imager observations of solar wind-driven ULF auroral pulsations, Geophys. Res. Lett., 35, L16101. doi:10.1029/2008GL034953.
19. Liou K, & Takahashi K (2013), Observations of field line resonance with global auroral images. Journal of Atmospheric and Solar: Terrestrial Physics, 105-106, 152–159.

https://doi.org/10.1016/j.jastp.2013.09.005.

20. Liou K, & Sibeck DG (2014), Study of a global auroral Pc5 pulsation event with concurrent ULF waves, Geophys. Res. Lett., 41, 6547–6555. doi:10.1002/ 2014GL060755.
21. Liou K, & Sibeck DG (2018), Dawndusk auroral oval oscillations associated with high-speed solar wind. Journal of Geophysical Research: Space Physics, 123, 600–610. https://doi.org/10.1002/ 2017JA024527
22. Liu, J. J., H. Q. Hu, D. S. Han, T. Araki, Z. J. Hu, Q. H. Zhang, H. G. Yang, N. Sato, A. S. Yukimatu and Y. E. Ebihara, Decrease of auroral intensity associated with reversal of plasma convection in response to an interplanetary shock as observed over Zhongshan station in Antarctica, J. Geophys. Res., 116, A03210, doi:10.1029/2010JA016156, 2011.
23. Liu, J. J., H. Q. Hu, D. S. Han, Liu Y., Q. H. Zhang, A. S. Yukimatu, (2013), Optical and SuperDARN radar observations of duskside shock aurora over Zhongshan Station, Advances in Polar Science, 24, doi: 10.3724/SP.J.1085.2013.00060.
24. McFadden J, Carlson C, Larson D, Bonnell J, Mozer F, Angelopoulos V, Glassmeier K-H, Auster U (2008), The THESIS ESA first science results and performance issues, Space Sci. Rev., 141, 477–508. doi:10.1007/s11214-008-9433-1.
25. Mende SB, Harris S, Frey H, Angelopoulos V, Russell C, Donovan E, Jackel B, Greffen M, Peticolas L (2008), The THEMIS array of ground-based observatories for the study of auroral substorms, Space Sci. Rev., 141, 357–387.
26. Milan S, Sato N, Ejiri M, Moen J (2001), Auroral forms and the field-aligned current structure associated with field line resonances, J. Geophys. Res., 106 (A11), 25,825–25,833. doi:10.1029/2001JA900077.
27. Nishitani, N., Ruohoniemi, J. M., Lester, M., et al., 2019. Review of the accomplishments of mid-latitude Super Dual Auroral Radar Network (SuperDARN) HF radars, Prog. Earth Planet Sci., 6, 27, doi:10.1186/s40645-019-0270-5.
28. Oguti T, Nakamura R, Yamamoto T (1987), Oscillations in drifts of auroral patches, J. Geomagn. Geoelectr., 39, 609–624.
29. Rostoker G & Sullivan B (1987), Polarization characteristics of Pc5 magnetic pulsations in the dusk hemisphere, Planet. Space Sci., 35, 429–438.
30. Ruohoniemi JM, Greenwald RA (1998) The response of high-latitude convection to a sudden southward IMF turning. Geophys Res Lett 25:2913–2916
31. Saka O, Hayashi K, Klimushkin DY, Mager PN (2014), Modulation of auroras by Pc5 pulsations in the dawn sector in association with reappearance of energetic particles at geosynchronous orbit, J. Atmos. Sol. Terr. Phys., 110-111, 1–8.
32. Samson J C, Cogger LL, Pao Q (1996), Observations of field line resonances, auroral arcs, and auroral vortex structures, J. Geophys. Res., 101(A8), 17,373–17,383. doi:10.1029/96JA01086.
33. Samson JC, Rankin R, Tikhonchuk VT (2003), Optical signatures of auroral arcs produced by field line resonances: comparison with satellite observations and modeling, Annales Geophysicae, 21,

933-945.

34. Sandholt PE, Lockwood M, Oguti T, Cowley SWH, Freeman KSC, Lybekk B, Egeland A, Willis DM (1990), Midday auroral breakup events and related energy and momentum transfer from the magnetosheath, J. Geophys. Res., 95, 1039–1060.
35. Sato N, Kadokura A, Tanaka Y, Nishiyama T, Hori T, Yukimatu AS (2015), Omega band pulsating auroras observed onboard THEMIS spacecraft and on the ground, J. Geophys. Res. Space Physics, 120, 5524- 5544, doi:10.1002/2015JA021382.
36. Sato N, Yukimatu AS, Tanaka Y, Hori T(2017), Morphologies of omega band auroras, Earth, Planets and Space 69:103 DOI 10.1186/s40623-017-0688-1.
37. Shepherd SG, Greenwald RA, Ruohoniemi JM (1999) A possible explanation for rapid, large-scale ionospheric responses to southward turnings of the IMF. Geophys Res Lett 26:3197–3200
38. Southwood DJ (1974), Some features of field line resonances in the magnetosphere, Planet. Space Sci., 22, 483– 491.
39. Tanaka Y-M, Ebihara Y, Saita S, Yoshikawa A, Obana Y, Weatherwax AT (2012), Poleward moving auroral arcs observed at the South Pole Station and the interpretation by field line resonances, J. Geophys. Res., 117, A09305. doi:10.1029/2012JA017899.
40. Tsyganenko NA, & Sitnov MI (2005), Modeling the dynamics of the inner magnetosphere during strong geomagnetic storms, J. Geophys. Res., *110*, A03208. https://doi.org/10.1029/2004JA010798.
41. Xu B-L, Samson JC, Liu WW, Creutzberg F, Hughes TJ (1993), Observations of optical aurora modulated by resonant Alfvén waves, J. Geophys. Res., 98(A7), 11,531–11,541. doi:10.1029/93JA00435.
42. Yamamoto T, et al (1988), Auroral activities and long-period geomagnetic pulsations: 1 Pc5 pulsations and concurrent auroras in the dawn sector, J. Geomagn. Geoelectr., 40, 553–569.

Table

Due to technical limitations, table 1 png is only available as a download in the Supplemental Files section.

Figures

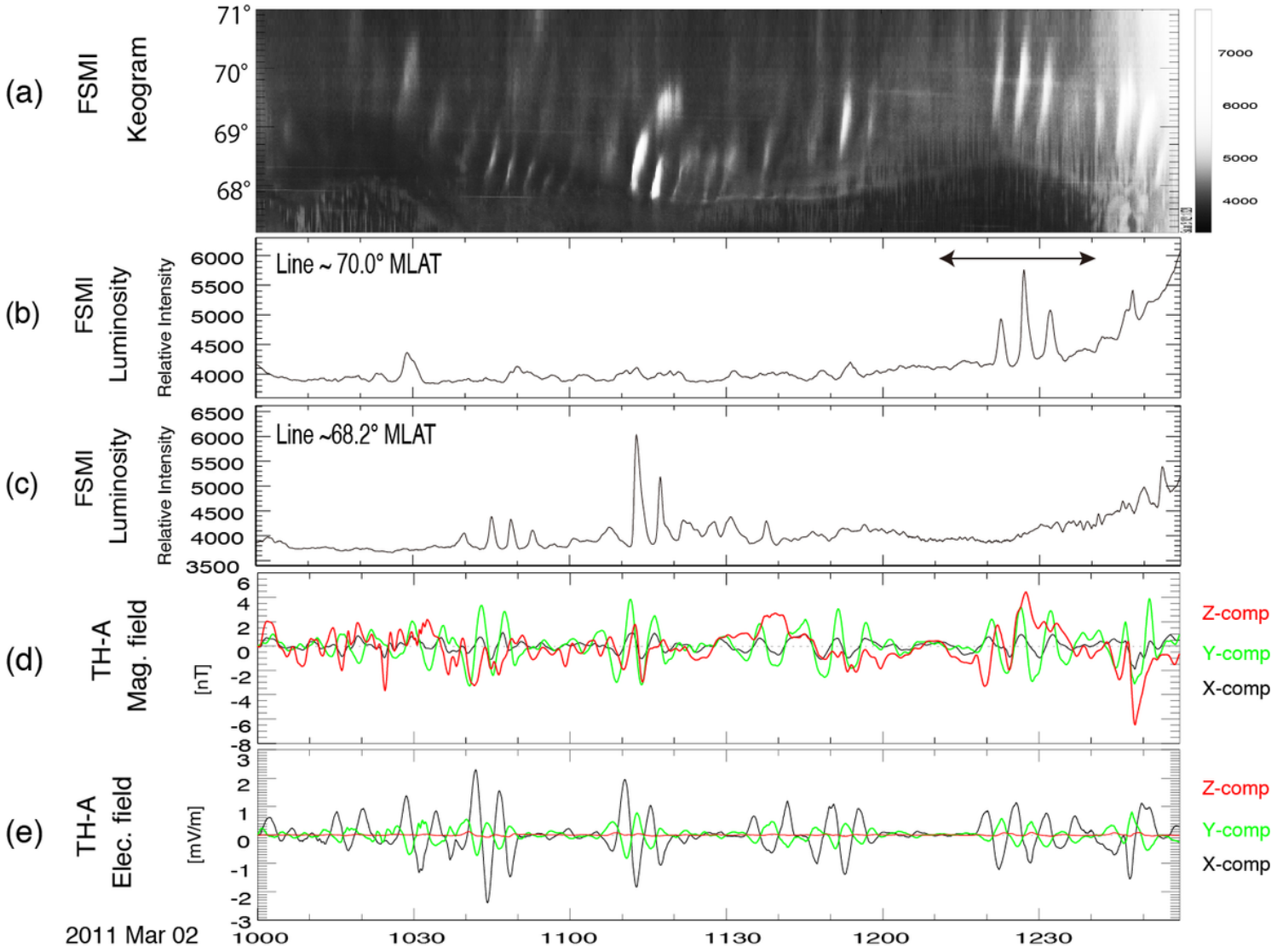

Figure 1

(a) Keogram observed at Fort Smith (FSMI). Luminosity at lines (b) ~70.0° MLAT and (c) ~68.2° MLAT. (d) Magnetic and (e) electric field variations with a bandpass filter of 60–600 s observed onboard TH-A.

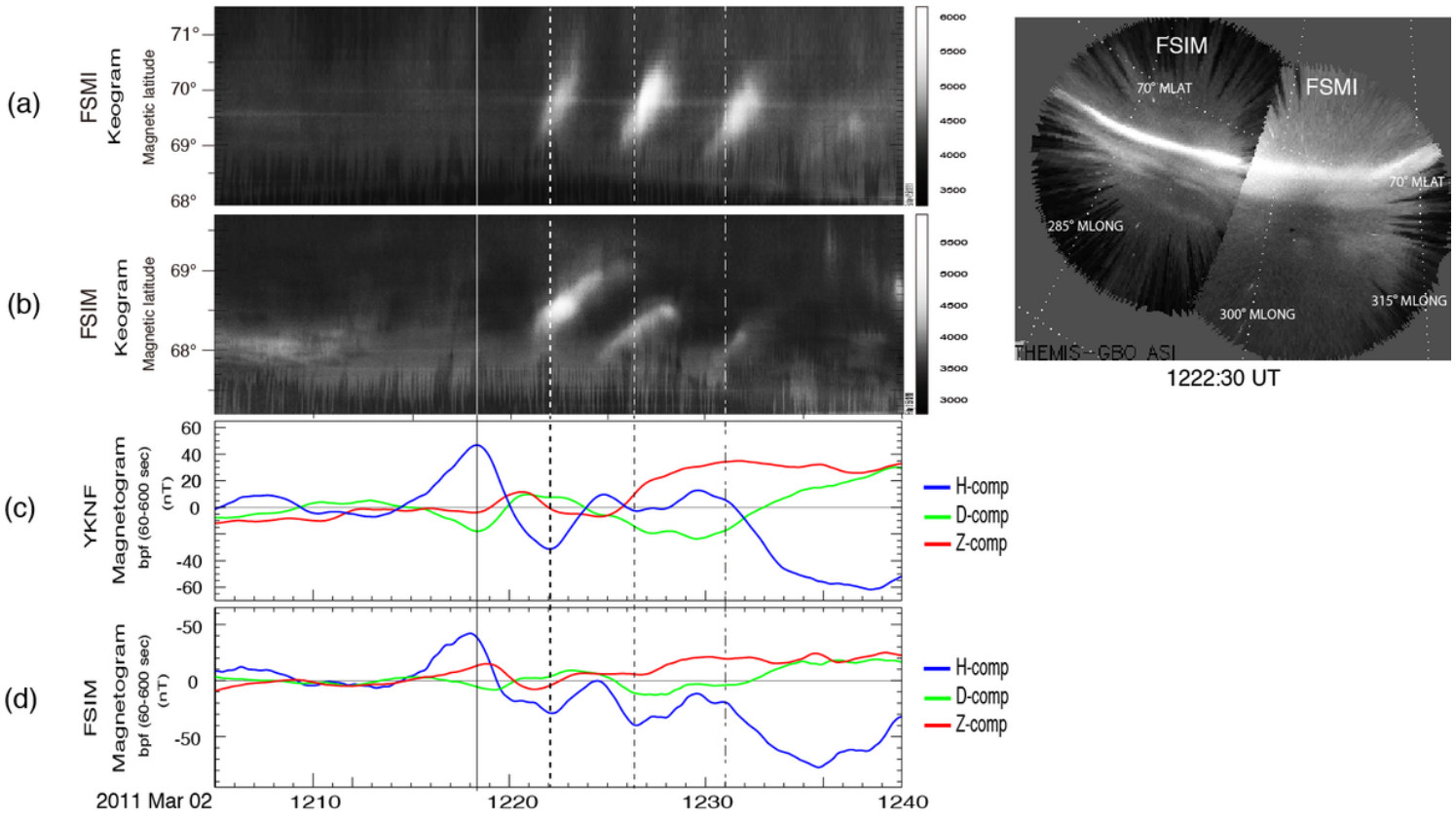

Figure 2

Pc5 PMMA pulsations observed at FSMI and FSIM in Canada and magnetogram observed at YKNF and FSIM.

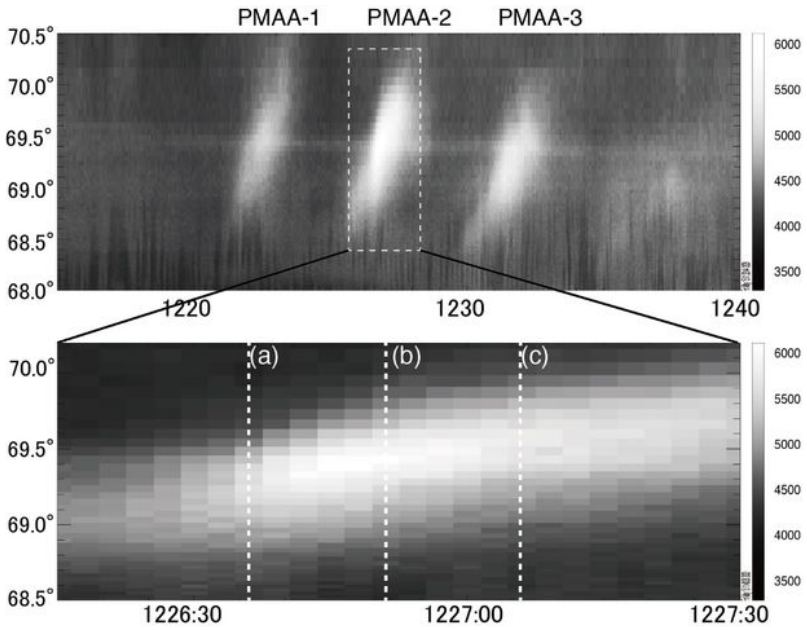

Fig 3a

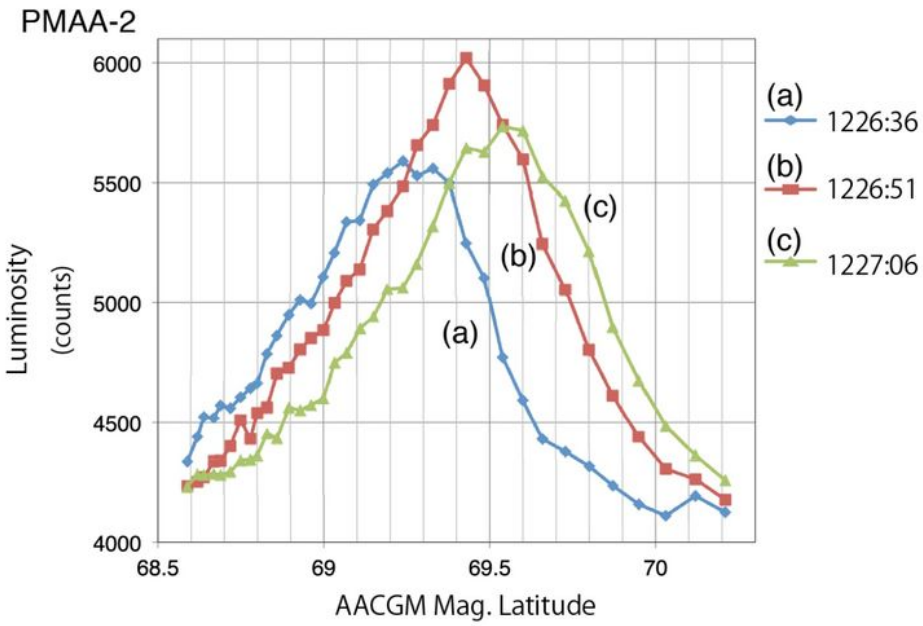

Fig 3b

Figure 3

3a: Keogram observed at FSMI (upper panel) and the expanded keogram (bottom panel) both in time and latitude in the dotted square as marked at the top panel. 3b: Luminosity distribution with magnetic latitude at the time intervals of (a), (b), and (c) as shown in the vertical line at the bottom panel of "Figure 3a" during the PMAA-2.

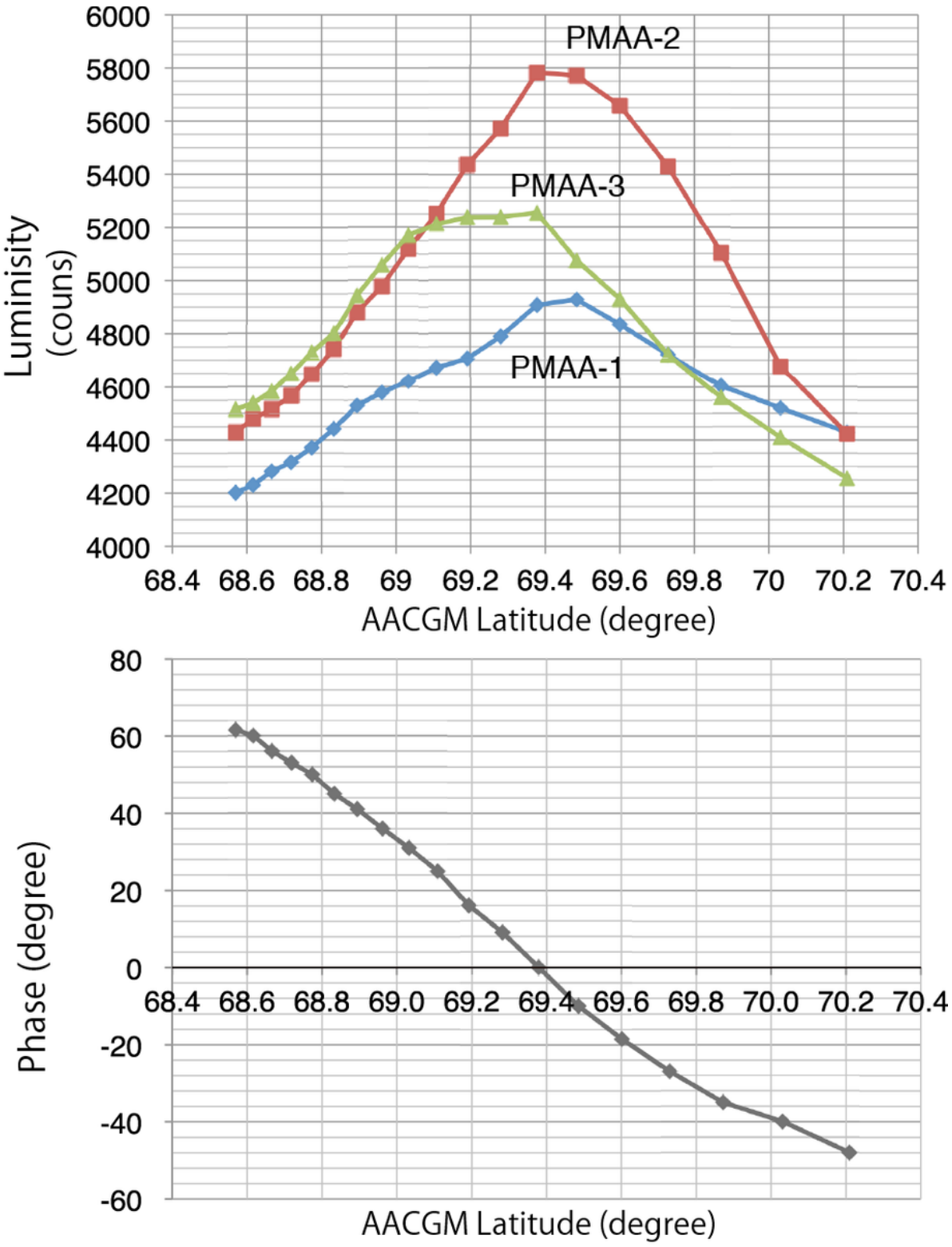

Figure 4

(Upper panel) Latitudinal distribution of the maximum auroral luminosity at each sampling time on the keogram for PMAA-1, PMAA-2, and PMAA-3. (Bottom panel) Relative phase on luminosity oscillation of PMAA versus magnetic latitude. The phase "zero" is located at the latitude of the luminosity maximum of PMAA-2.

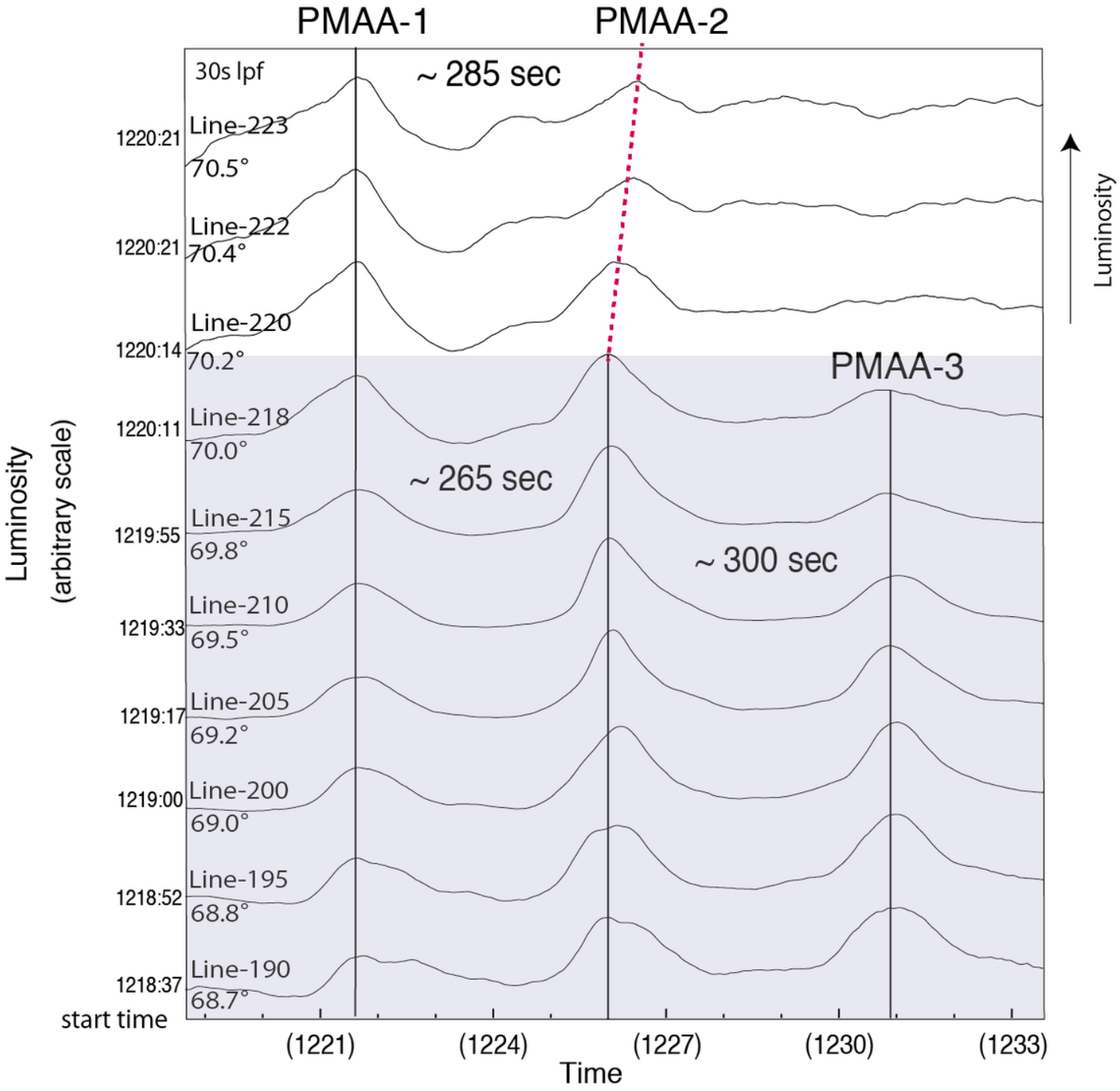

Figure 5

Luminosity plots with time for 10 luminosity lines. Plots are arranged as that the luminosity maximum time at each line during the PMAA-1 was fitted at the same moment by shifting the start time.

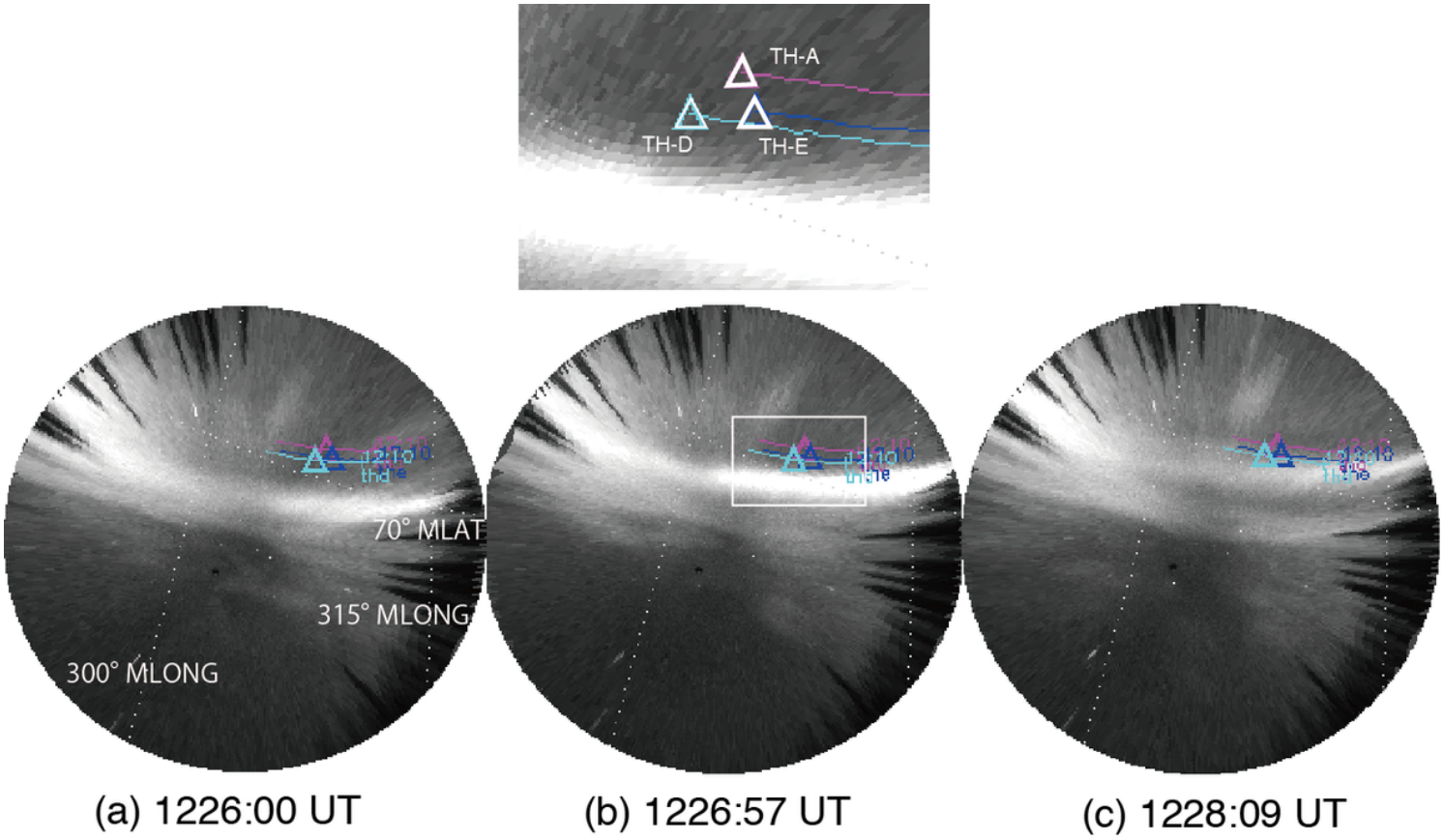

Figure 6

Auroral snapshot images observed at FSMI from the initial phase of the auroral arc pulsation (a) to the maximum intensity phase (c) and footprints of TH-A, TH-D, and TH-E spacecraft at a 110 km altitude (top right).

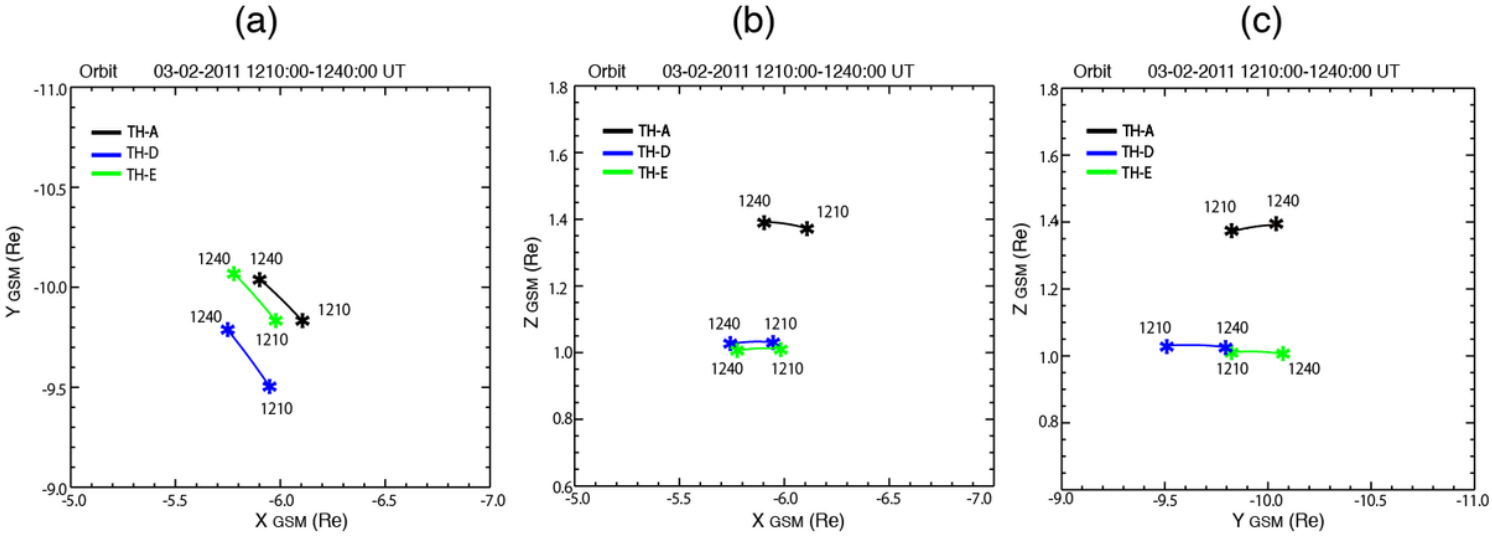

Figure 7

Spacecraft orbit configurations in three different planes (X-Y, X-Z, and Y-Z) in the GSM coordinate system.

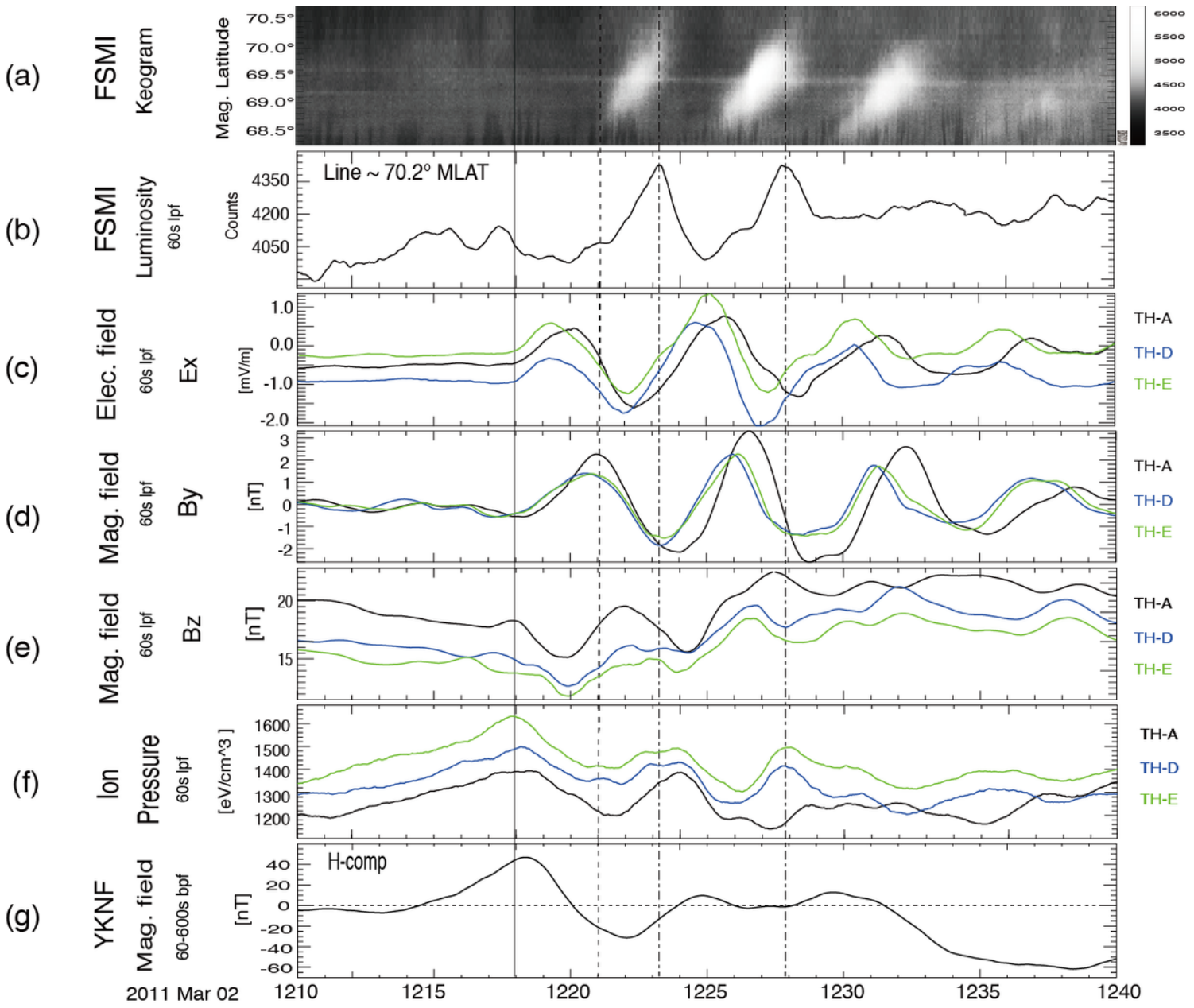

Figure 8

Auroral keogram (a) and relative intensity of the luminosity at line ~ 70.2° MLAT with a low pass filter of 60 s (b) observed at FSMI; TH-A, D and E spacecraft data of Ex (c), By (d), Btotal (e), and ion pressure (f) displayed with band-pass filter of 60–600 s; (g) H component of the ground-based magnetogram at YKNF.

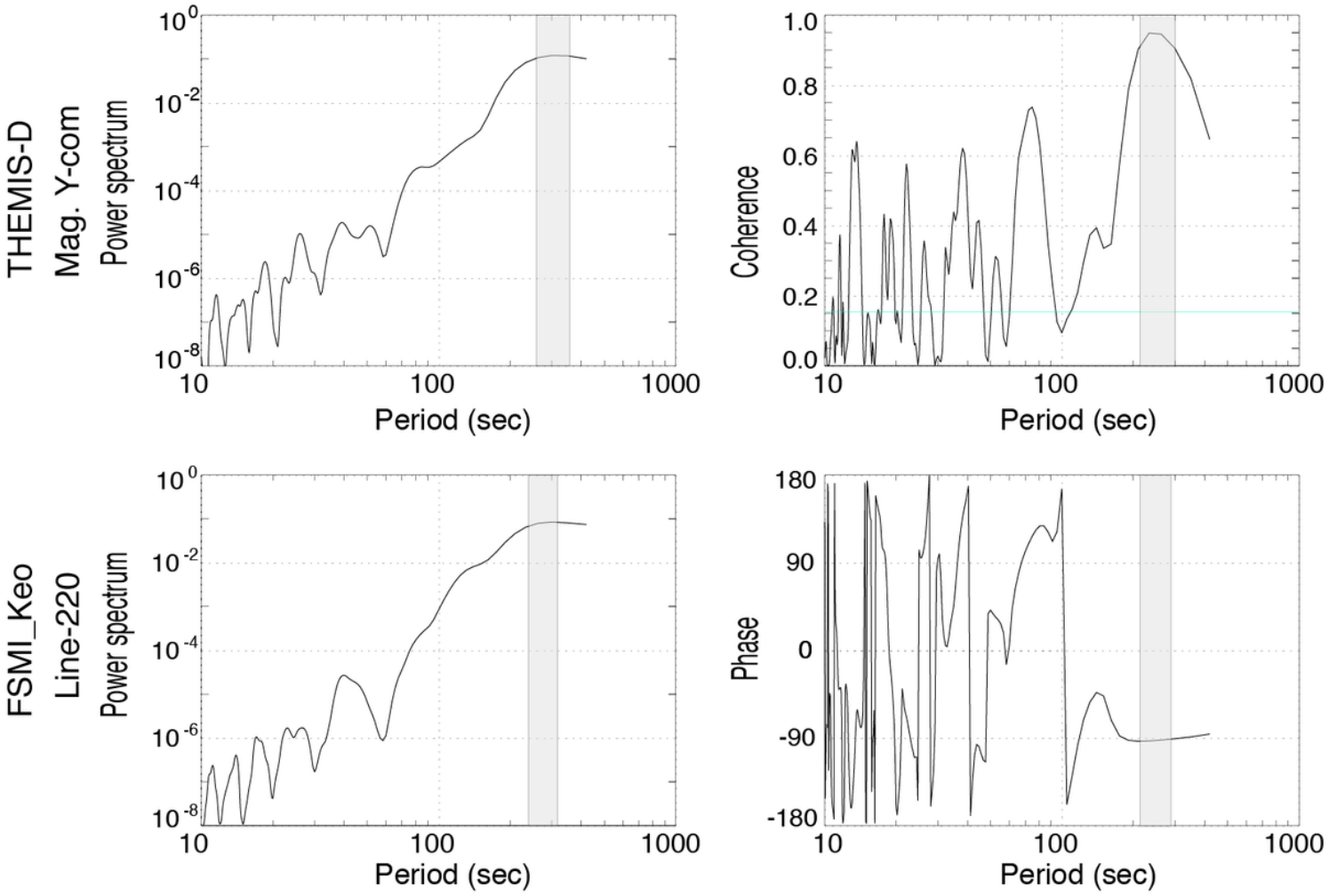

Figure 9

Left: power spectra of the Y component of the magnetic field oscillations at TH-D (upper panel) and the luminosity pulsations at line 220 (lower panel). Right: coherency (upper panel) and phase difference (lower panel) between the two data.

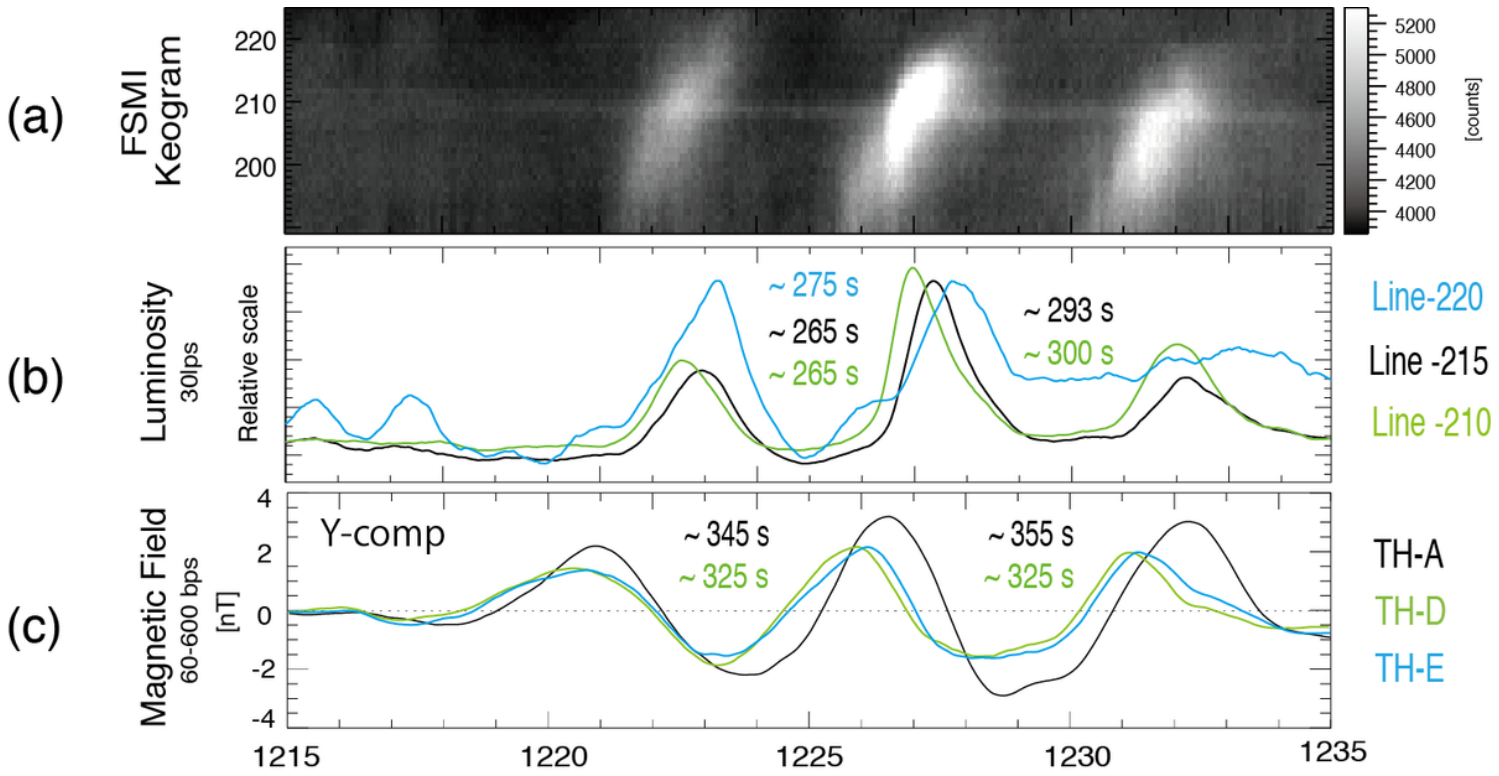

Figure 10

(a) auroral keogram observed at FSMI (upper panel), (b) relative intensity of the auroral keogram at line 210, 215, and 220, and (c) Y component of magnetic field observed at TH-A, TH-D, and TH-E.

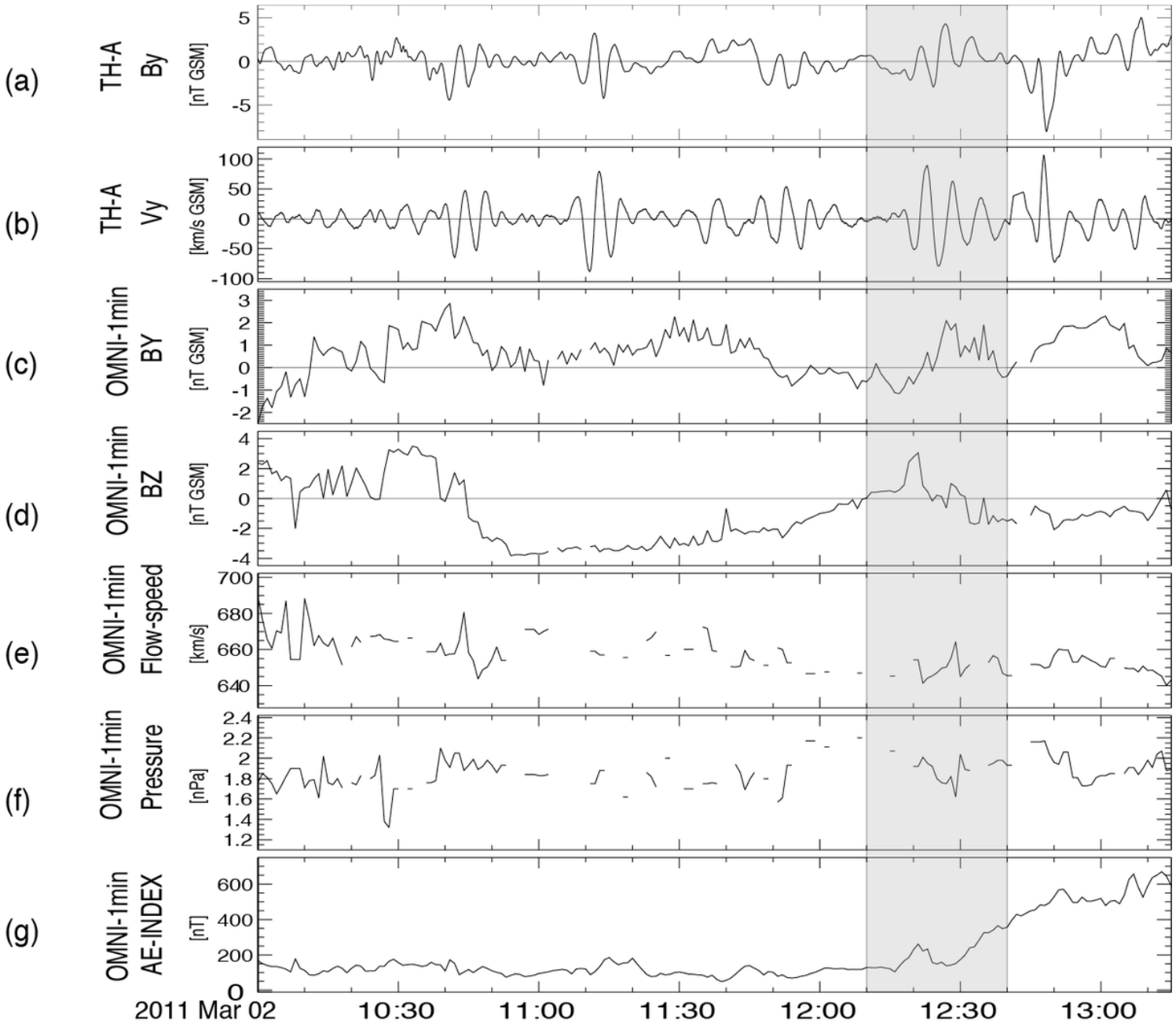

Figure 11

Y component of the magnetic field (a) and Y component of flow velocity (b) observed onboard TH-A. OMNI 1-minute data of IMF By (c), Bz (d), flow speed (e), and pressure (f). (g) AE index.

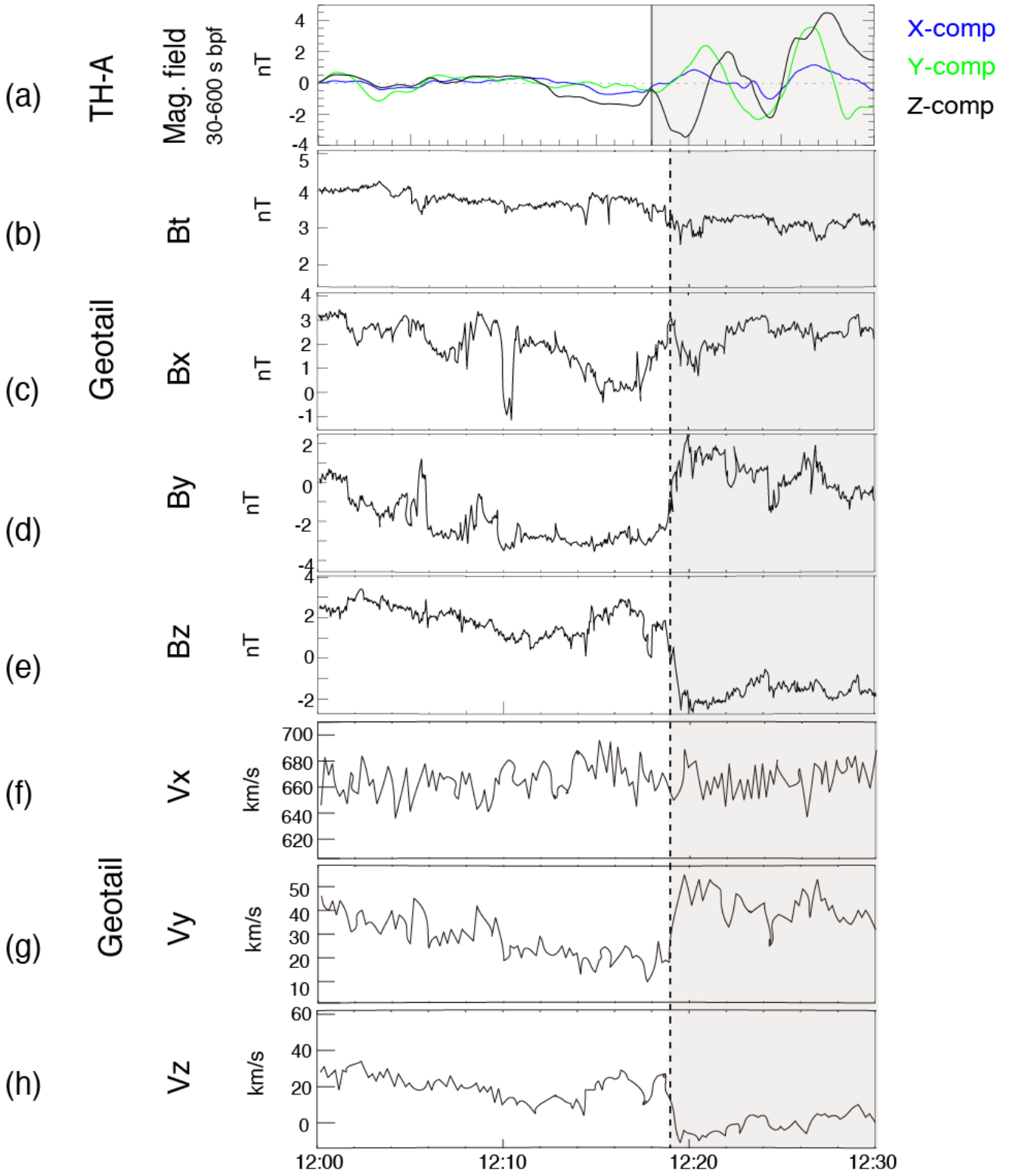

Figure 12

X, Y, and Z component of the magnetic field at TH-A (a), Geotial data of Btotal (b), Bx (c), By (d), Bz (e), Vx (f), Vy (g), and Vz (h).

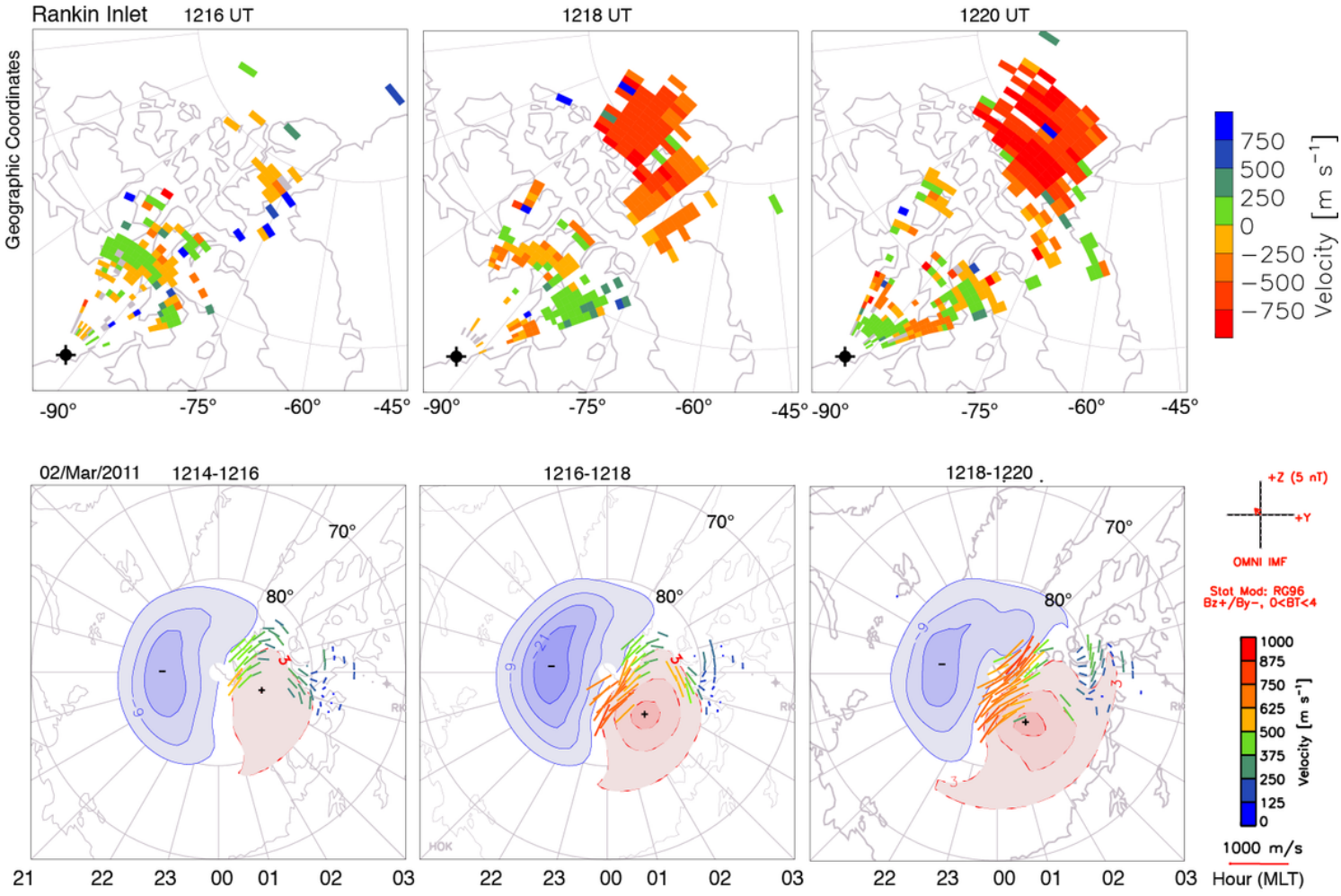

Figure 13

Line of site velocity at the polar cap SuperDARN radar obtained at Rankin Inlet.

Supplementary Files

This is a list of supplementary files associated with this preprint. Click to download.

- Table1.png
- Graphycalabstract19.08.19.png
- ReferenceDataT96andT05modelTHA.pdf
- MovieS1.mp4
- Additionalfiles.text.docx